Solid Earth, 13, 497–518, 2022
https://doi.org/10.5194/se-13-497-2022

Solid Earth Open Access EGU

Rare earth elements associated with carbonatite–alkaline complexes in western Rajasthan, India: exploration targeting at regional scale

Malcolm Aranha[1], Alok Porwal[1,2], Manikandan Sundaralingam[3], Ignacio González-Álvarez[4,2], Amber Markan[3], and Karunakar Rao[3]

[1]Centre of Studies in Resources Engineering (CSRE), Indian Institute of Technology Bombay, Mumbai, 400076, India
[2]Centre for Exploration Targeting, University of Western Australia, Crawley, 6009, Australia
[3]Datacode, Nagpur, 440033, India
[4]Commonwealth Scientific and Industrial Research Organisation (CSIRO), Mineral Resources, Kensington, 6151, Australia

Correspondence: Malcolm Aranha (malcolmaranha@iitb.ac.in)

Received: 29 August 2021 – Discussion started: 24 September 2021
Revised: 23 January 2022 – Accepted: 25 January 2022 – Published: 14 March 2022

Abstract. A two-stage fuzzy inference system (FIS) is applied to prospectivity modelling and exploration-target delineation for rare earth element (REE) deposits associated with carbonatite–alkaline complexes in the western part of the state of Rajasthan in India. The design of the FIS and selection of the input predictor map are guided by a generalised conceptual model of carbonatite–alkaline-complex-related REE mineral systems. In the first stage, three FISs are constructed to map the fertility and favourable geodynamic settings, favourable lithospheric architecture for fluid transportation and favourable shallow crustal (near-surface) emplacement architecture, respectively, for REE deposits in the study area. In the second stage, the outputs of the above FISs are integrated to map the prospectivity of REE deposits in the study area. Stochastic and systemic uncertainties in the output prospectivity maps are estimated to facilitate decision-making regarding the selection of exploration targets. The study led to the identification of prospective targets in the Kamthai–Sarnu-Dandeli and Mundwara regions, where detailed project-scale ground exploration is recommended. Low-confidence targets were identified in the Siwana ring complex region, north and northeast of Sarnu-Dandeli, south of Barmer, and south of Mundwara. Detailed geological mapping and geochemical sampling together with high-resolution magnetic and radiometric surveys are recommended in these areas to increase the level of confidence in the prospectivity of these targets before undertaking project-scale ground exploration. The prospectivity-analysis workflow presented in this paper can be applied to the delineation of exploration targets in geodynamically similar regions globally, such as Afar province (East Africa), Paraná–Etendeka (South America and Africa), Siberia (Russia), East European Craton–Kola (eastern Europe), Central Iapetus (North America, Greenland and the Baltic region) and the pan-superior province (North America).

1 Introduction

According to the International Union of Pure and Applied Chemistry (IUPAC), the term rare earth elements (REEs) includes yttrium (Y), scandium (Sc) and the lanthanides (lanthanum, La; cerium, Ce; praseodymium, Pr; neodymium, Nd; promethium, Pm; samarium, Sm; europium, Eu; gadolinium, Gd; terbium, Tb; dysprosium, Dy; holmium, Ho; erbium, Er; thulium, Tm; ytterbium, Yb; and lutetium, Lu). Because of their increasing use in environment-friendly high-technology industries, REEs are widely considered as the resources of the future (e.g. Goodenough et al., 2018; Wall, 2021). Most countries have classified REEs as "critical minerals and metals" because of their strategic importance and the projected gap between their future demand and supply (Goodenough et al., 2018; González-Álvarez et al., 2021, and references therein).

In spite of significant efforts into developing technology for recovering and recycling REEs from discarded devices (Binnemans et al., 2013), geological resources are likely to remain the primary sources of REEs in the foreseeable future (Goodenough et al., 2018). Several classification schemes for REE deposits have been proposed by different workers based on geological associations and settings, for example, Chakhmouradian and Wall (2012), Jaireth et al. (2014), Wall (2014), Goodenough et al. (2016), Verplanck and Hitzman (2016), and Simandl and Paradis (2018). In general, REE deposits can be broadly classified into those formed by high-temperature (magmatic and hydrothermal) processes and those formed by low-temperature (mechanical and residual concentration) processes (e.g. Wall, 2021). Although the majority of Indian production of REEs comes from low-temperature deposits such as regolith-hosted and heavy-mineral placers (IBM yearbook 2018, 2019), the bulk of geological resources are in high-temperature magmatic deposits, particularly those associated with carbonatites (e.g. Bayan Obo, Inner Mongolia, China; Mount Weld, Western Australia; Maoniuping, South China; Mountain Pass, USA; González-Álvarez et al., 2021 and references therein).

India ranks sixth in terms of production of REEs and fifth in terms of resources (USGS, 2021). All of India's production comes from monazite-bearing beach sands along the eastern and western coasts (IBM yearbook 2018, 2019). Since India has 29 out of the total 527 globally reported carbonatite occurrences (Woolley and Kjarsgaard, 2008a), there is significant latent potential for carbonatite-related REE deposits in the country. Currently, there are no studies available, at least in the public domain, on systematic delineation of prospective REE exploration targets in India.

Mineral prospectivity modelling is a widely used predictive tool for identifying exploration target areas for mineral exploration. Implemented in a GIS environment, it involves the integration of "predictor maps" that represent a set of mappable exploration criteria for the targeted deposit type. Typically, conceptual mineral systems models are used to identify exploration criteria (Porwal and Kreuzer, 2010; Porwal and Carranza, 2015). The integration is done through either linear or non-linear mathematical functions (Bonham-Carter, 1994; Porwal, 2006; Porwal and Carranza, 2015). Depending on how the model parameters are estimated, that is, whether based on training data comprising attributes of known deposits or on expert knowledge, these models are classified as data-driven or knowledge-driven. Data-driven approaches require a sizeable sample of known deposits of the targeted deposit type for estimating the model parameters, while knowledge-driven approaches use expert knowledge for estimating model parameters. Fuzzy-logic-based approaches are the most widely used knowledge-driven approaches to prospectivity modelling. These approaches have evolved from the Prospector (Duda et al., 1978, 1979, 1980), which was the earliest knowledge-based expert system that utilised fuzzy operators in a Bayesian network (Porwal et al., 2015).

The outputs of both data-driven and knowledge-driven prospectivity models are subject to two types of uncertainties (Porwal et al., 2003; Lisitsin et al., 2014), namely, systemic (or epistemic) and stochastic (or aleatory). Systemic uncertainties arise from the incomplete understanding of the geological process involved in the formation of the mineral deposit, leading to imperfect models. Stochastic uncertainties arise from the limitations of the primary and derivative processed datasets, including the algorithms used to derive them. These uncertainties are the results of inaccuracy or imprecision in measurements and observations, data interpolations, and inconsistent data coverage (Porwal et al., 2003; McCuaig et al., 2009; Lisitsin et al., 2014). However, most published prospectivity modelling studies do not specifically deal with uncertainties in model outputs.

There are very few published studies on REE prospectivity modelling. Ekmann (2012) published a study of REEs in coal deposits in the United States. In one of the first GIS-based prospectivity modelling studies for REEs, Aitken et al. (2014) used a fuzzy-logic-based model to delineate prospective targets for pegmatite-, carbonatite- and vein-hosted REEs in the Gascoyne region of Western Australia. This study was part of a larger multi-commodity prospectivity study of the Gascoyne Province. Sadeghi (2017) carried out a regional-scale GIS-based prospectivity analysis for REEs in the Bergslagen district of Sweden, targeting iron-apatite- and skarn-associated deposits using the weights of evidence and weighted-overlay models. Bertrand et al. (2017) used database querying to analyse the prospectivity for REEs as by-products in known mineral deposits in Europe. In a recent study, Morgenstern et al. (2018) analysed the potential of REEs in New Zealand using a multi-stage fuzzy inference system (FIS).

This contribution describes the first systematic and comprehensive prospectivity modelling exercise aimed at identifying exploration targets for REE associated with carbonatite–alkaline complexes in western Rajasthan, India (Fig. 1). Although it is a well-established carbonatite province that is widely considered prospective for REE deposits, only a single REE deposit has been identified in the province so far. We employ fuzzy inference system (FIS), which is a knowledge-driven artificial intelligence technique, to identify and delineate prospective targets for REEs (except Pm and Sc; Pm is an unstable element and Sc is not an element sourced from carbonatite–alkaline complexes) in the study area. The inputs to the FIS were identified based on a generalised mineral systems model for carbonite–alkaline-complex-related REEs, which was further used to guide the design of the FIS. To support decision-making regarding the delineated targets, uncertainties in the output model were also estimated. The prospectivity-analysis workflow presented in this paper can be applied to other geodynamically similar regions (with mantle-plume-related intra-

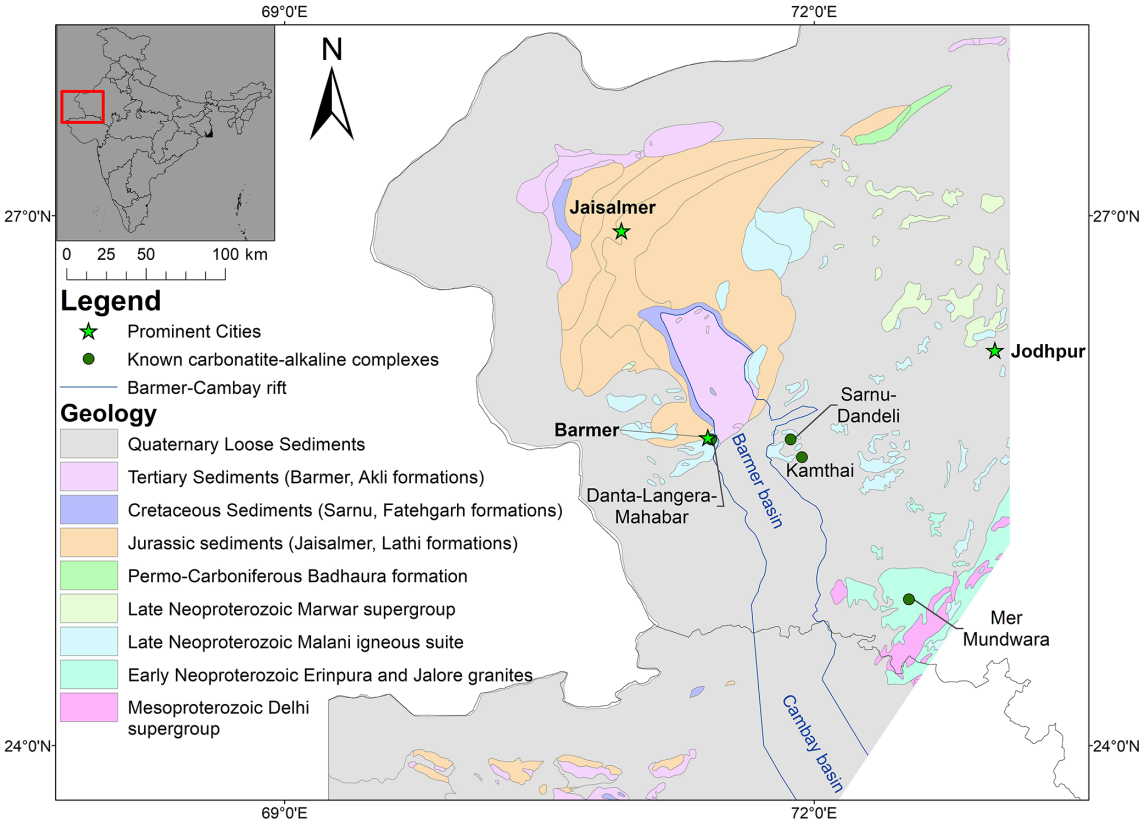

Figure 1. Geological map of the study area with known carbonatite–alkaline complexes.

continental extensional settings) globally for exploration targeting, e.g. in eastern Africa, South and North America, Russia, eastern Europe, Greenland and the Baltic region.

2 Geological setting of the study area

The study area is located in the state of Rajasthan in northwestern India (Fig. 1). This area was chosen because it is a known major carbonatite province of India, and well-integrated public domain datasets are available. Geologically, the study area contains igneous and sedimentary formations ranging in age from the Neoproterozoic to Holocene. Neoproterozoic Erinpura and Jalore granites, along with a few outcrops of the Mesoproterozoic Delhi Supergroup, occur in the southeastern part of the study area (Fig. 1). The eastern part of the study area comprises extrusive and intrusive igneous rocks belonging to the Neoproterozoic Malani Igneous Suite that is mostly covered by a thick horizon of Holocene wind-blown sand. Sedimentary sequences belonging to the Late Neoproterozoic Marwar Supergroup, Jurassic Jaisalmer, Cretaceous Sarnu–Fatehgarh, Tertiary Barmer (Palaeocene) and Akli (Eocene), and Quaternary Uttarlai formations (Pleistocene to Holocene) (Roy and Jakhar, 2002; Ramakrishnan and Vaidyanadhan, 2008; Singh et al., 2016) occur in the central and western parts around Barmer and Jaisalmer towns (Fig. 1).

Carbonatite–alkaline complexes of the Cretaceous age occur in the Mer-Mundwara area in the eastern part of the study area and the Sarnu-Dandali area in the central part of the study area (Fig. 1; Table A1). The Mer-Mundwara carbonatite–alkaline complex intrudes the Neoproterozoic Erinpura Granite and displays a characteristic ring structure, wherein the alkaline-mafic rock suites form two ring structures and a dome (Pande et al., 2017). Carbonatites mainly occur in the form of linear dykes at Mer-Mundwara. The Sarnu-Dandeli complex covers a relatively large area on the eastern shoulder of the Barmer Basin. The carbonatites occur mainly as scattered plugs and dykes that are covered by Quaternary sand, intruding the Neoproterozoic Malani igneous suite and the Cretaceous Sarnu formation (Vijayan et al., 2016; Sheth et al., 2017). The Sarnu-Dandeli complex also includes more minor occurrences of carbonatites in the Danta-Langera-Mahabar and Kamthai areas. The Kamthai plug is considered to be highly prospective for REEs (Bhushan and Kumar, 2013).

The study area is dissected by the Barmer rift, which continues southwards through the state of Gujarat into the Cambay Basin. The Barmer rift is a failed, roughly north–south-trending, extensional intracratonic rift (Fig. 1) that was ac-

tive during the Late Cretaceous to Eocene (Dolson et al., 2015). A long-lasting extensional regime predating the Deccan volcanism existed in northwestern India, peaking with the Seychelles rifting at the Cretaceous–Paleogene boundary and the emplacement of the main phase of Deccan volcanics at ca. 65 Ma (Devey and Stephens, 1992; Allegre et al., 1999; Chenet et al., 2007; Collier et al., 2008; Ganerød et al., 2011; Bladon et al., 2015a, b). The well-preserved Cretaceous carbonatite–alkaline complexes of the study area represent a young carbonatite magmatism episode ($\sim$ 68 Ma) that is coeval with the initial magmatism of the Deccan Large Igneous Province (LIP) and is related to the India–Seychelles break-up and northward drifting of India over the Réunion mantle plume (Devey and Stephens, 1992; Basu et al., 1993; Simonetti et al., 1995; Allegre et al., 1999; Ray and Pande, 1999; Ray and Ramesh, 1999; Ray et al., 2000; Chenet et al., 2007; Collier et al., 2008; Sheth et al., 2017; Chandra et al., 2018).

3 Datasets and methodology pipeline

The public domain geoscience datasets used in the study, which include geological, geophysical, topographic and satellite data, were mainly sourced from the Bhukosh portal (https://bhukosh.gsi.gov.in/Bhukosh/MapViewer.aspx, last access: 10 October 2019) of the Geological Survey of India (GSI). Table 1 summarises the sources, scales and other details about the individual datasets. Figure 2 depicts the outline of the methodology used in this study, which is discussed in detail in the next sections.

4 Mineral systems model for carbonatite–alkaline complex related REE deposits

In this study, we used the generalised conceptual model of carbonatite–alkaline-complex-related REE mineral systems developed by Aranha et al. (in review) based on the framework proposed by McCuaig and Hronsky (2014). Figure 3 illustrates the main features of the model. The main components of the mineral systems are compiled in Table 2 and briefly summarised in the following paragraphs.

Fertile source region. Metasomatised pockets of the subcontinental lithospheric mantle (SCLM) are considered to be the fertile source regions for carbonatite–alkaline complexes (Jones et al., 2013) as well as REE deposits associated with these complexes, as the processes of metasomatism also cause enrichment of REE and other incompatible elements (Zheng, 2012, 2019). The metasomatism of the SCLM involves one of the following processes: (1) lithospheric subduction into the SCLM (no. 1 in Fig. 3 and Table 2; Duke, 2009; Duke et al., 2014; Goodenough et al., 2016); (2) anatexis-induced mixing of subducting crustal units with the SCLM (no. 2 in Fig. 3 and Table 2; Jones et al., 2013 and references therein); or (3) metasomatism induced by ascending mantle plumes (no. 3 in Fig. 3 and Table 2; Simonetti et al., 1995, 1998; Bell and Tilton, 2002; Bell and Simonetti, 2010; Ernst and Bell, 2010).

Geodynamic setting. Carbonatite–alkaline complexes and related REE deposits generally occur in extensional intracontinental rifts and large igneous provinces (LIPs) (no. 4, 5, 6 in Fig. 3 and Table 2; Woolley and Kjarsgaard 2008a; Woolley and Bailey, 2012; Pirajno, 2015; Simandl and Paradis, 2018). Extensional tectonic settings and associated LIPs are manifestations of mantle plumes (Simonetti et al., 1995, 1998; Bell and Tilton, 2002; Bell and Simonetti, 2010; Ernst and Bell, 2010), which also induce metasomatism of the SCLM. As a result, fertile source regions of, and favourable geodynamic setting for, REE deposits related to the carbonatite–alkaline complex are interlinked.

Architecture. Carbonatite–alkaline complexes and related REE mineral systems derive fluids from the SCLM through large-scale permeable networks of trans-lithospheric structures. Most carbonatite–alkaline complexes are found spatially associated with crustal-scale faults, rifts and shear zones at regional scales (Ernst and Bell, 2010; Woolley and Bailey, 2012; Pirajno, 2015; Simandl and Paradis, 2018; Spandler et al., 2020). Therefore, lithosphere-scale structures form favourable plumbing structures for carbonatite–alkaline-complex-related REE deposits (no. 7 in Fig. 3 and Table 2). Upper crustal faults, shallow discontinuity structures and joints serve as pathways for focussing fluids to near-surface levels and also form structural traps (no. 8 in Fig. 3 and Table 2; Ernst and Bell, 2010; Skirrow et al., 2013; Jaireth et al., 2014).

The reaction of the carbonatite–alkaline magma with the country-rock results in the formation of Ca and Mg silicates and removal of CO_2, dissolved P and F (Skirrow et al., 2013; Jaireth et al., 2014). The above reactions may cause REEs to deposit in silicate minerals along the country-rock interface (Anenburg and Mavrogenes 2018; Anenburg et al., 2020). Enrichment of incompatible elements such as REEs, U, Th, Nb, Ba, Sr, Zr, Mn, Fe and Ti in the fluids occur due to liquid immiscibility, especially in liquids rich in alkalis which promote REE solubility (no. 10, 13, 14, 15, 16, 17, 18, 19 in Fig. 3 and Table 2; Cordeiro et al., 2010; Skirrow et at., 2013; Jaireth et al., 2014; Pirajno, 2015; Mitchell, 2015; Chakhmouradian et al., 2015; Stoppa et al., 2016; Poletti et al., 2016; Giovannini et al., 2017; Simandl and Paradis, 2018; Spandler et al., 2020; Anenburg et al., 2020). Carbonatite–alkaline complexes are often enriched in ferromagnesian minerals that cause well-defined magnetic and gravity anomalies (no. 9 in Fig. 3 and Table 2; Gunn and Dentith, 1997; Thomas et al., 2016). Fenitisation often enriches country rocks in K and Na (no. 12 in Fig. 3 and Table 2; Le Bas, 2008; Elliott et al., 2018). In alkali-rich intrusions, LREEs are retained in the primary carbonatite while HREEs tend to concentrate in fenites, particularly K-fenites, whereas in silica-rich or alkali-poor intrusions, HREEs remain in the

Table 1. A list of primary data available for the study area.

Primary data	Resolution/scale	Source
Geological map	1 : 50 000	GSI, accessed in October 2019
Structural map	1 : 50 000	GSI, accessed in October 2019
Total magnetic intensity (TMI)	75 m	GSI, accessed in October 2019
Ground Gravity	1 : 1 000 000	Reddi and Ramakrishna (1988), accessed in October 2019
World Gravity Map 2012 (WGM2012) Bouguer gravity	0°2′	Bonvalot et al. (2012); accessed in November 2019
ETOPO1 1 arcmin Global Relief Model	0°1′	Amante and Eakins (2009), Bonvalot et al. (2012); accessed in November 2019
Shuttle Radar Topography Mission (SRTM) topography	0°0′3″	Geosoft seeker; accessed in October 2019
Structural lineament map	1 : 250 000	GSI, accessed in October 2019
Known carbonatite occurrences		Literature review; Table A1
Known prospects		GSI and Atomic Minerals Directorate (AMD) (2020)

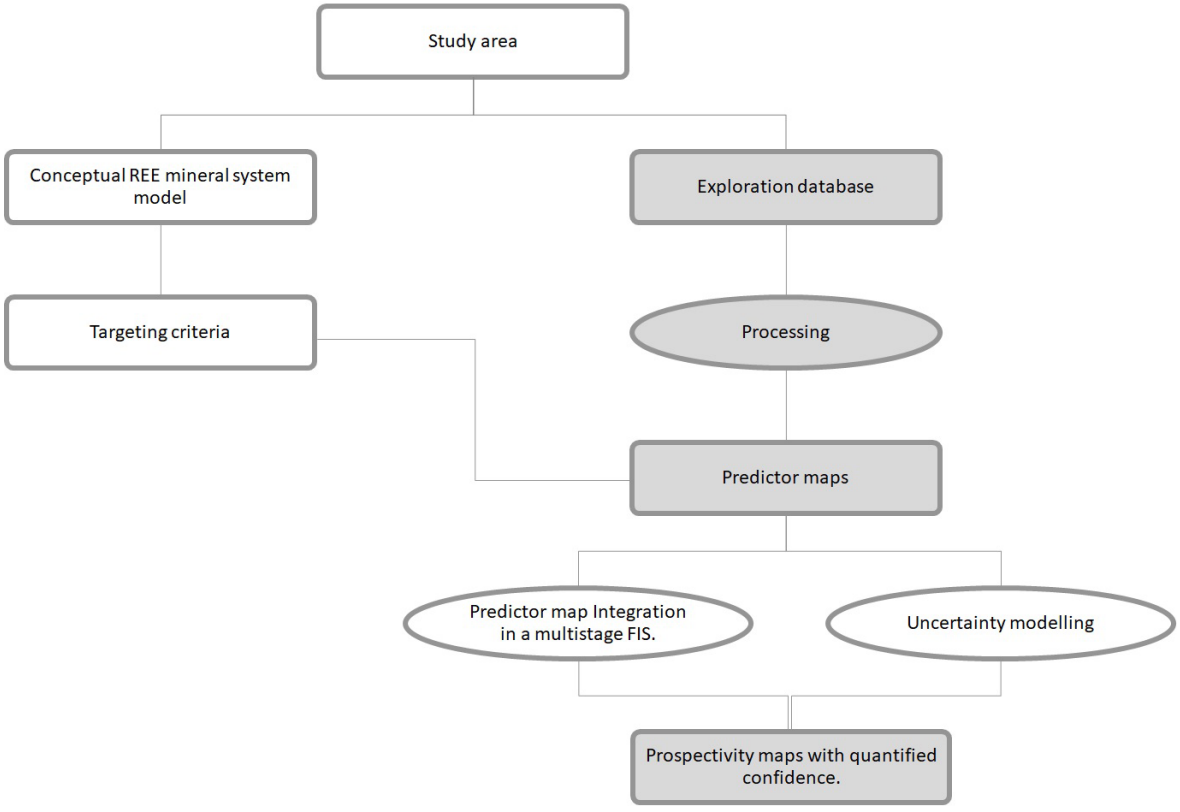

Figure 2. Flow chart depicting the methodology. Rectangular boxes contain generated objects, and oval boxes contain processes used for creating the objects. Shaded boxes indicate the objects and processes created and implemented in a GIS, respectively.

carbonatite (Anenburg et al., 2020). Size and HREE/LREE concentration of the fenites halo are major proxies.

REE mineralisation in the carbonatites can be in the form of primary REE-bearing minerals (e.g. Mountain Pass, Mariano, 1989; Castor, 2008; Verplanck and Van Gosen, 2011; Van Gosen et al., 2017) or by secondary hydrothermal activity, including in situ replacement, or from late magmatic fluid phases evolved from the carbonatite magmas (Verplanck and Van Gosen, 2011; Skirrow et at., 2013; Jaireth et al., 2014; Van Gosen et al., 2017). Primary REE-bearing cumulates include perovskite, pyrochlore, apatite and calcite, while late-stage REE-bearing minerals include bastnäsite, parisite and synchysite that form from the redistribution of soluble primary phases such as ancylite, burbankite and carbocernaite (no. 24 in Table 2; Verplanck and Van Gosen, 2011; Skirrow et al., 2013; Van Gosen et al., 2017; Andersen et al., 2017; Anenburg et al., 2020; Kozlov et al., 2020).

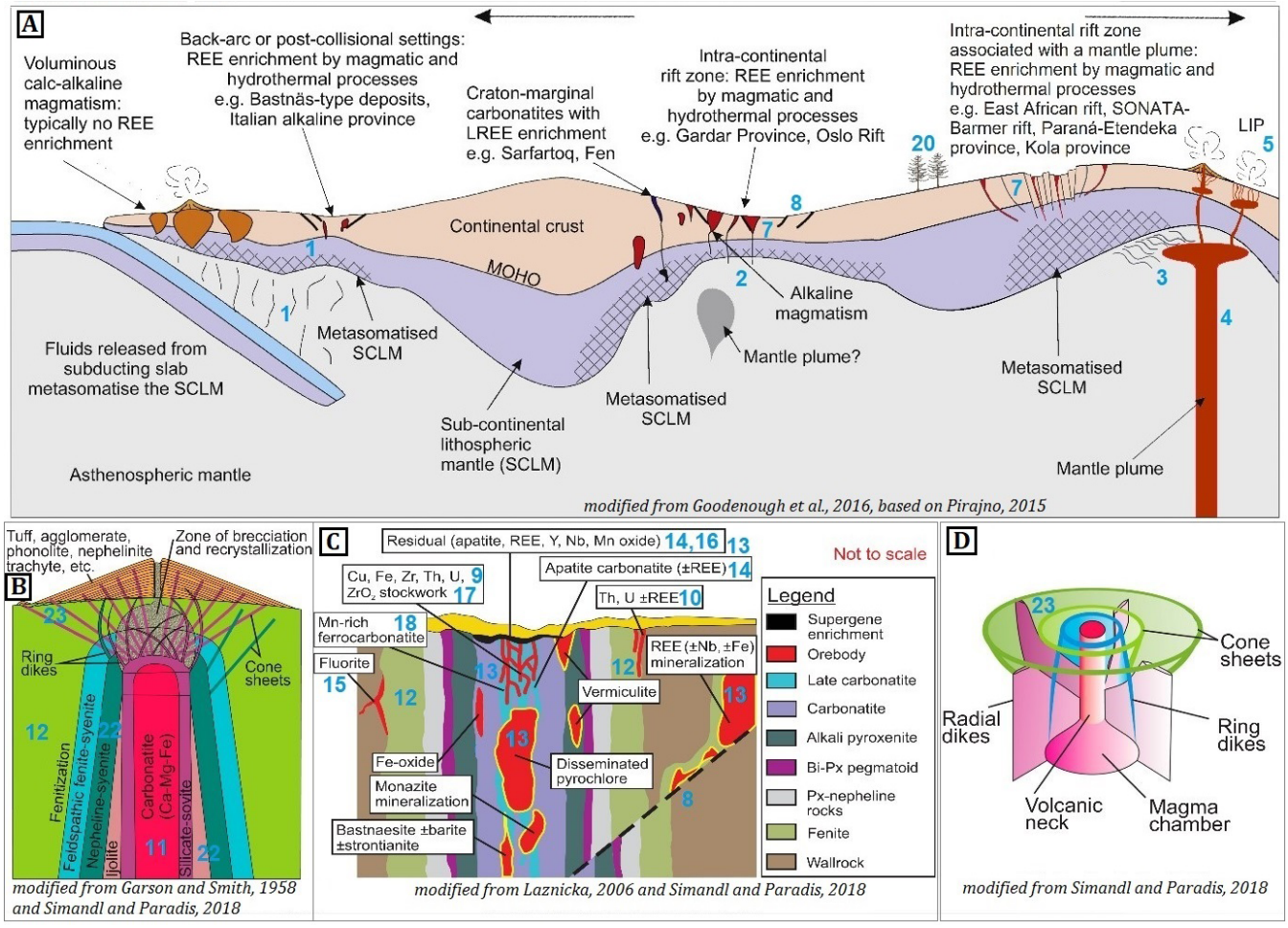

Figure 3. Idealised genetic model of a carbonatite–alkaline-complex-related REE mineral system (adapted from Aranha et al., 2022) cross-referenced to processes listed in Table 2 through the numbers in blue. Panel **(a)** depicts the fertility and geodynamic setting along with the transport architecture on a regional scale. Panels **(b–d)** focus on the emplacement architecture at the camp-to-prospect-scale. Panel **(b)** shows the idealised geometry of the intrusion and the relation of carbonatites and associated alkaline rocks and fenitisation. Panel **(c)** presents the near-surface structural architecture and the spatial distribution of associated rocks. Panel **(d)** displays the idealised geometry of a carbonatite–alkaline intrusion and the relationship between the magma chamber, ring dykes, cone sheets and radial dykes.

5 Targeting criteria and predictor maps

The above conceptual model for carbonatite–alkaline-related REE mineral systems was translated into a "targeting model", which is a compilation of processes whose responses can be mapped directly or indirectly from the publicly available datasets for the study area listed in Table 1. The targeting model was used to identify regional-scale mappable targeting criteria for REE deposits in the study area (Table 3).

The mappable targeting criteria for REE deposits in the study area were represented in the form of GIS layers or predictor maps for inputting into the FIS. The details of the primary data, the algorithms, and GIS tools and techniques used to generate input predictor maps are provided in Table 3. Since there is a 1–2 orders of difference in the spatial resolution of the input datasets (ranging from ∼ 100 m for airborne magnetic data to ∼ 10 km for ground gravity data), we chose a trade-off grid cell size of 3 km for generating the input predictor maps. The same grid cell size was used for prospectivity analysis. This grid cell size corresponded to the size of typical carbonatite–alkaline-complex occurrences in the study area.

6 FIS-based prospectivity modelling

The predictor maps were integrated using FIS (Fig. 4) to generate REE prospectivity maps of the study area. The theory of the FIS-based modelling approach and implementation for mineral prospectivity modelling is provided by Porwal et al. (2015) and Chudasama et al. (2016). Several open-source software packages and libraries for imple-

Table 2. Conceptual REE mineral systems model (adapted from Aranha et al., under review). The index numbers correlate to the numbers in blue in Fig. 3.

Setting/process	No.	Targeting criteria	Spatial proxies
Fertility			
Mantle metasomatism and low-degree partial melting	1	Subduction of crust	Subduction zones throughout geological history
	2	Decompressional melting of mantle and crust due to rifting (crustal thinning)	Rift zones
	3	Metasomatism driven by a rising mantle plume	Trace of mantle plume
Geodynamic setting and triggers			
Continental rifts (rising mantle plume)	4	Trace of mantle plumes based on plate	Trace of mantle plume through time
	5	tectonics through indicative magmatism	LIP
	6	Major global tectonic events – super-continental break-ups	Plate reconstruction models – rifting
Architecture transport			
Migration of magma along existing or new architecture	7	Crustal scale discontinuities	Rift structure Deep-crust-penetrating faults
Architecture emplacement			
Magma emplacement under structural traps	8	Near-surface network of faults	Shallow intersecting faults
Carbonatite magma emplacement: Concentration of minerals with a strong magnetic response and contrasting density from the country rocks	9	Anomalous high signatures in geophysical data	Anomalous high signatures in magnetic and gravity data
Concentration of incompatible radioactive elements	10	High radioactivity due to U and Th enrichment	High response in radiometric maps due to U and Th Anomalous high signatures of U and Th in geochemical data
Hosted by or strongly associated with Ca or Mg carbonate rocks (carbonatites)	11	High concentrations of Ca and Mg	Anomalous high signatures in geochemical data.
Sodic and potassic fenitisation	12	Enrichment of K and Na in the surrounding rocks; size and HREE/LREE of the fenites halo	High response in radiometric maps due to K. HREE/LREE map
Emplacement of incompatible elements in primary carbonatite or secondary carbonatitic veins	13	Enrichment of REEs	Anomalous high signatures in geochemical data.
	14	P_2O_5,	
	15	F, Cl and CO_3;	
	16	Nb	
	17	Ba, Sr, Zr	
	18	Mn	
	19	Ti	
Biogeochemical indicators: absorption of REEs and related elements by plants growing over a potential deposit	20	Abundance of Ba, Sr, P, Cu, Co, La, Ce, Pr, Nd, Sm, Dy, Fe, Nb, Ta, U and Y against the background value in the leaves and twigs of the plants and in the Humus.	Plant/humus anomaly maps
Selective absorption of specific wavelengths of the electromagnetic spectrum (Boesche et al., 2015; Neave et al., 2016; Zimmermann et al., 2016)	21	Characteristic absorption features in remotely sensed spectral images	REE concentration maps derived from remotely sensed spectral images
Carbonatites are commonly spatially associated with alkaline silicates (85 %; Woolley and Kjarsgaard, 2008a, b) and in some cases with ultramafic and felsic silicate igneous rocks	22	Known alkaline intrusions	Mapped intrusions in geological maps
Concentric zoning of carbonate rocks along with magnetic minerals (magnetite) (Gunn and Dentith, 1997; Thomas et al., 2016)	23	Circular outline	Circular features in topographic and geophysical data
Variation in mineralogy in REE-bearing minerals and associated alkaline suite of rocks are indicators of emplacement depth as well as erosional level and, therefore, mineralisation potential	24	Variation in rock units of the alkaline rock suite and/or variation of REE minerals	Individual rock and mineralogical units in detailed lithological and mineralogical profiles

menting FIS are available in the public domain (e.g. FISDeT, Castellano et al., 2017; FisPro, R package "FuzzyR"; Python library "fuzzy expert"). However, in the present study, we used the commercial software Fuzzy Logic Toolbox of MathWorks® to implement the model. The concepts and theory of fuzzy logic, as well as the procedures for designing and implementing FIS using the Fuzzy Logic Toolbox, are explained in detail in the documentation that can be freely accessed at https://mathworks.com/help/fuzzy/fuzzy-inference-process.html.

The modelling was implemented in the following steps.

1. Fuzzification of numeric predictor maps. In the first step, all numeric predictor maps (e.g. the predictor map showing distance to structural lineaments) were converted into fuzzy predictor maps (e.g. proximity to structural lineaments) using membership functions such as linear, piecewise linear (trapezoidal) or Gaussian (Table 4). However, the output fuzzy membership values of a predictor map are dependent on the shape of the membership function used, which in turn is dependent on the mathematical parameters that define the function, e.g. mean and standard deviation for

Table 3. Targeting model, spatial proxies and steps used to derive the predictor maps of the three components of the REE mineral system in northwestern India.

SNO	Spatial proxy (predictor maps)	Procedures used to generate the predictor map	Rationale
Fertility and geodynamic setting			
1	Barmer rift (Euclidean distance to rift)	Rift outline traced from the vertical derivative of reduced to pole (RTP) magnetic data and extrapolated using lineament map.	Rift represents crustal extension caused by a rising mantle plume. It marks a zone of extension and deep permeable faults that facilitate magma flow. Vertical derivative of magnetic data enhance the responses of near-surface shallow features (Gönenç, 2014) where the rift zone is likely to be widest. The Barmer rift is assumed to be the trace of the mantle plume.
2	Deccan LIP (Euclidean distance to the Deccan LIP)	Extracted from the geological map.	Mantle plumes result in the formation of large igneous provinces, and thus, LIPs can be used to demarcate the zone of influence of the mantle plume. Carbonatites are known to be associated with mantle plumes.
Transport architecture component			
3	Regional lineaments (Euclidean distance to lineaments derived from magnetic and gravity data continued upwards to (1) 2 km, (2) 5 km, (3) 10 km and (4) 20 km.)	RTP magnetic, ground gravity and WGM2012 gravity data were continued upwards to 2 km, 5 km, 10 km and 20 km, respectively, followed by calculating the total horizontal derivative of the 12 images (four each from magnetic, WGM2012 and ground gravity data). Euclidean distance was calculated to the lineaments extracted from the respective images after edge-enhancements, and combined using fuzzy "AND" operator.	Crustal-scale structures such as shear zones and crust-penetrating faults are excellent conduits for magma transportation. Such features manifest as linear trends on magnetic data (Porwal, 2006). Magnetic and gravity data continued upwards to 2 km, 5 km, 10 km and 20 km show responses from progressively deeper crustal sources (Jacobsen, 1987; Pawlowski, 1995); thus, these lineaments are considered to continue to such deeper levels.
4	Inferred faults (Euclidean distance to inferred faults)	Euclidean distance to inferred faults and structural lineaments calculated.	Faults are favourable conduits for fluid flow.
5	Barmer rift (Euclidean distance to rift)	As above (1)*	A rift represents a zone of large-scale extension and comprises deeply penetrating faults that serve as conduits for magma migration.
Emplacement architecture component			
6	Post-Cambrian non-felsic intrusive bodies (Euclidean distance to post-Cambrian, non-felsic intrusives)	Post-Cambrian, non-felsic intrusive rocks were extracted from the geological map.	Non-felsic intrusions (mainly alkaline intrusions) associated with carbonatites represent a magmatic episode that triggered, or were part of alkaline and carbonatitic magmatic activity.
7	Deccan LIP (Euclidean distance to the Deccan LIP)	As above (2)*	The carbonatite–alkaline complexes were emplaced in the Deccan LIP (Pande et al., 2017; Sheth et al., 2017; Chandra et al., 2018).
8	Inferred faults (Euclidean distance to inferred faults)	As above (4)*	Faults focus fluid flow and act as structural traps, particularly where they intersect.
9	Circular features (Euclidean distance to circular features derived from magnetic, gravity and topographic data)	Total Horizontal derivative was calculated of the RTP and the gravity images, and their respective 2 km and 5 km upward continued maps, followed by extraction of circular features (Holden et al., 2011). Circular features were also extracted from topographic datasets. All derived circular features were overlaid and integrated using the fuzzy "AND" operator.	Intrusive carbonatites contain concentric zoning of carbonate rocks with variable concentrations of magnetite that cause concentric or roughly oval anomalies (Gunn and Dentith, 1997). The horizontal derivative of RTP magnetic data and gravity data and their progressive upward continuations show responses from progressively deeper crustal sources (Jacobsen, 1987; Pawlowski, 1995); thus, these circular features are considered to continue to deeper levels. Exposed carbonatite–alkaline ring complexes typically exhibit a circular outline in topographic data.
10	Shallow Lineaments (Euclidean distance to surficial lineaments derived from (1) magnetic data (2) WGM2012 and (3) ground gravity data)	Euclidean distance was calculated to lineaments extracted from the vertical derivative of (1) RTP magnetic data, (2) WGM2012 and (3) ground gravity data, after edge-enhancements. These maps were integrated using the fuzzy "AND" operator.	Shallow, surficial, higher-order, local faults and joints aid in focussing the fluids to near-surface levels and can also serve as structural traps. Such features manifest as linear trends on geophysical data (Porwal, 2006). Vertical derivative of magnetic data reveal responses from near-surface sources (Gönenç, 2014); thus, these lineaments are considered to be near-surface.
11	Intersections of shallow lineaments (Euclidean distance to intersections of surficial lineaments)	Points of intersections were extracted of lineaments derived from the vertical derivative of (1) RTP magnetic data, (2) WGM2012 and (3) ground gravity data.	Intersections of near-surface lineaments can serve as structural traps.
12	High magnetic anomalies (Magnetic anomaly map)	Analytical signals of magnetic data were calculated to exaggerate anomalous signatures	Carbonatites are often enriched in magnetic minerals such as magnetite that exhibit high magnetic susceptibility. Analytical signals are useful for localising anomalies over their sources at lower magnetic latitudes (Rajagopalan, 2003; Keating and Sailhac, 2004).

* These maps were used as proxies for several different components, as explained under the rationale column.

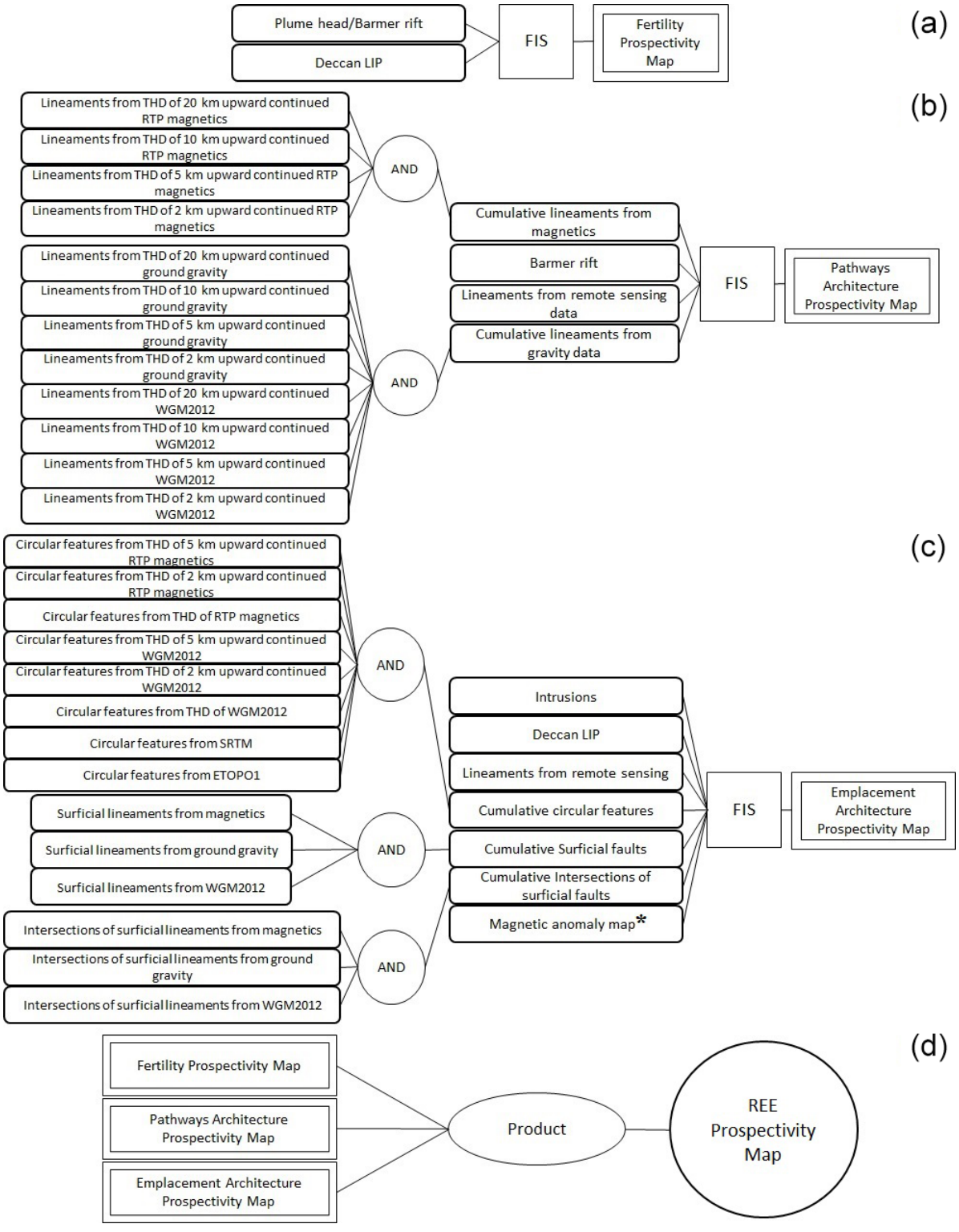

Figure 4. The multi-stage FIS for REE prospectivity mapping in the study area. **(a)** FIS for generating fuzzy prospectivity maps for fertile sources and favourable geodynamics settings. **(b)** FIS for generating fuzzy prospectivity maps for favourable lithospheric architecture for transportation of REE-enriched carbonatite–alkaline magma. **(c)** FIS for generating fuzzy prospectivity maps for favourable shallow crustal (near-surface) architecture for emplacement of carbonatite–alkaline complexes. **(d)** Second-stage FIS combines the above three prospectivity maps obtained from the first stage and generates the final outputs. * All the input maps in **(a–c)** are Euclidean distance maps, except for the magnetic anomaly map in **(c)**.

Table 4. Input variables, linguistic values and types of membership functions.

Input predictor map	Linguistic values	Types of membership function
Premise variables		
· FERTILITY/GEODYNAMIC SETTING		
1. Euclidean distance to Barmer rift[1].		
2. Euclidean distance to Deccan LIP[1].	Proximal	Piece-wise linear (Trapezoidal)[2]
· TRANSPORT ARCHITECTURE		
3. Euclidean distance to lineaments derived from magnetic data.		
Euclidean distance to lineaments derived from gravity data.		
4. Euclidean distance to inferred faults[1].		
5. Euclidean distance to Barmer rift[1].	Intermediate	Gaussian[3]
· EMPLACEMENT ARCHITECTURE		
6. Euclidean distance to post-Cambrian, non-felsic intrusions.		
7. Euclidean distance to Deccan LIP[1].		
8. Euclidean distance to inferred faults[1].		
9. Euclidean distance to circular features.	Distal	Piece-wise linear (Trapezoidal)[2]
10. Euclidean distance to shallow lineaments.		
11. Euclidean distance to intersections of shallow lineaments.		
	High	Piece-wise linear (Trapezoidal)[2]
12. Magnetic anomaly map.	Intermediate	Gaussian[3]
	Low	Piece-wise linear (Trapezoidal)[2]
Consequent variables		
· Fertility and Geodynamic setting prospectivity	High	Linear[4]
· Transport architecture prospectivity	Intermediate	Gaussian[3]
· Emplacement architecture prospectivity	Low	Linear[4]

1. These maps were used as predictor maps for more than one component. However, different parameters were used for the membership functions for different components.
2. A piece-wise linear function comprises several linear functions with different slopes. The ones used in this study are trapezoidal functions. This function returns a constant fuzzy membership value of 1 (definitely proximal) up to a certain distance. Beyond this distance, the degree of proximity decreases linearly with distance up to a certain distance, and hence fuzzy membership decreases accordingly. Beyond this distance, it returns a fuzzy membership value of 0 (definitely not proximal). It may be noted that for "Distal" the function outputs are vice versa.
3. A Gaussian function allots a high membership function to the average value (centre of the peak of the function). As a result, this function was used for the 'intermediate' fuzzy sets.
4. The output (consequent) variables have been assigned linear membership functions to model the favourability on a linear scale

Gaussian functions and slope and intercept for linear functions.

Because there are insufficient known deposits to use as training data for optimising the fuzzy membership functions, we quantified uncertainty arising from using sub-optimal function parameters (termed "systemic uncertainty"; Porwal et al., 2003; Lisitsin et al., 2014). The algorithm utilising Monte Carlo simulations described by Lisitsin et al. (2014) and Chudasama et al. (2017) was used to estimate model uncertainties. In this approach, instead of using point values for the parameters of the fuzzy membership functions, we used beta-PERT distributions conforming to the possible variations of these point values. The beta is a bounded distribution that is widely used when there are no training data, and the only information available is the expert knowledge about the optimistic, most likely and pessimistic values (Johnson et al., 1995). The parameters of the beta functions (optimistic, most likely and pessimistic values) were assigned based on a geological evaluation of the decay of the influence of a targeting criteria with distance (Table 4). A series of Monte Carlo simulations were then carried out to estimate the values of the parameters at 10 %, 50 % and 90 % probability levels, which were respectively used to generate three fuzzy maps at 10 %, 50 % and 90 % probability levels for each predictor map.

However, the present work has not quantified other systemic uncertainties arising from the choice of the membership function, FIS structure, and choice of distribution.

2. FIS-based prospectivity modelling. In the second step, a multi-stage FIS was designed to replicate the geological reasoning used by an exploration geologist for delineating regional-scale exploration targets.

In the first stage, a series of FISs were developed to generate fuzzy prospectivity maps for individual components of the REE mineral systems by combining their respective fuzzy predictor maps. The FISs for fertility and geodynamic settings, whole lithosphere architecture and near-surface ar-

chitecture (Fig. 4) comprised 5, 8 and 11 fuzzy if–then rules, respectively, which are shown in Tables A2, A3 and A4, respectively. Since each predictor map was converted into three fuzzy maps at 10 %, 50 % and 90 % probability levels, the outputs of this step were three fuzzy prospectivity maps for each mineral systems component at 10 %, 50 % and 90 % probability levels.

In the second stage, the above three sets of fuzzy prospectivity maps were combined using the fuzzy product operator (Fig. 4D) to generate three REE prospectivity maps of the study area at 10 %, 50 % and 90 % probability levels.

3. Generation of confidence map. In the third step, stochastic uncertainties, which arise from the limitations of public-domain datasets and procedures used for generating the predictor maps, were quantified in terms of confidence values for each predictor map using the Sherman–Kent scale (Jones and Hillis, 2003; Kreuzer et al., 2008) as described by Porwal et al. (2003), González-Álvarez et al. (2010) and Joly et al. (2012). The confidence value for each predictor map was assigned based on the degree of representativeness of the predictor map, i.e. how well it represents the mineralisation process it seeks to map. A predictor map was assigned a high confidence value if it directly mapped the targeting criteria and a low confidence value if it indirectly mapped the response of the targeting criterion. The confidence factor also captured the fidelity and precision of the primary dataset from which the input was derived. The confidence factor for all predictor maps, along with the justifications, are given in Table 5. The output confidence map was generated by combining the confidence factors of different predictor maps using the same fuzzy inference systems that were used for prospectivity modelling.

Finally, the three REE prospectivity maps of the study area at 10 %, 50 % and 90 % probability levels were colour-coded blue to red and draped over the confidence map for viewing as 3D surface models. In the 3D surface models, the colours represented prospectivity (blue tones signify low prospectivity and red tones signify high prospectivity), and elevation represented confidence (depressions signify low confidence and elevations signify high confidence).

7 Results and discussion

In the first stage, the first FIS maps REE fertility and favourable geodynamic settings (Fig. 4a and Table A2) by delineating areas that are likely to be underlain by plume-metasomatised SCLM. Considering the size of a typical mantle plume, these areas are expected to be very large. The second FIS maps favourable lithospheric architecture for the transportation of REE-enriched carbonatite–alkaline magma (Fig. 4b and Table A3) and narrows down the target areas identified by the first FIS to areas that are proximal to trans-lithospheric structures. The target areas demarcated by the second FIS are also relatively large, as immense trans-lithospheric structures, such as the 600 km long Barmer–Cambay rift, are expected to have a large zone of influence. The third FIS maps favourable shallow crustal (near-surface) architecture for the emplacement of carbonatite–alkaline complexes (Fig. 4c and Table A4) and further narrows down the target area to camp-size areas that are controlled by near-surface higher-order structures. These individual FISs in the first stage rely on simple logic-based rules to integrate the individual predictor maps (Tables A2–A4). The rules were framed based on our understanding of the REE mineral system. The use of the "and" operator in the "if" parts of the rules defining high prospectivity ensured that a pixel would get a high prospectivity value only if it is proximal to predictor features on all predictor maps. Similarly, the use of the "or" operator in the "if" parts of the rules defining low prospectivity ensured that a pixel would get a low prospectivity even if it is distal to predictor features on any one of the predictor maps. As a result, the extents of the areas with background (low) prospectivity are maximised, and high-prospectivity zones are narrowed down efficiently.

In the second stage of the multi-stage FIS, the output prospectivity maps of the individual components were integrated using the fuzzy product operator, which calculates the mathematical product of all input predictor maps (Bonham-Carter, 1994; Porwal et al., 2015). Since the individual FIS output values range between 0 and 1, it decreases the final integrated prospectivity values. The final outputs are shown as continuous-scale (relative) prospectivity maps at 10 %, 50 % and 90 % probability levels draped over the confidence map in Fig. 5a–c.

Conjunctive interpretations of prospectivity maps and confidence maps can help in making decisions regarding follow-up exploration, as summarised in Table 6.

Along with the known Mundwara, Sarnu-Dandeli and Kamthai carbonatite occurrences, high prospectivity (orange-red colours in Fig. 5a–c) occurs in areas immediately surrounding Sarnu-Dandeli and Mundwara at high probability and confidence levels. These areas may represent branching conduits of the central carbonatite–alkaline complex intrusion. Geological mapping and direct detection studies are recommended in these locations.

Areas of moderate to high prospectivity at low probability levels are mapped over a circular region east of Sarnu-Dandeli (Fig. 5a and b; rectangle number 1) and also over an area just south of the circular region (within rectangle 1 in Fig. 5a–c). The circular region corresponds to the Siwana ring intrusion, which consists of alkali granites and rhyolites. The Siwana ring intrusion is part of the Neoproterozoic Malani LIP (Bhushan and Mohanty, 1988). However, the Siwana ring intrusion has low prospectivity at high probability (Fig. 5c; rectangle number 1), while the smaller area to its south consistently has high prospectivity at high probability and confidence levels. The high values may be caused by the consistent presence of lineaments in this region and the magnetic response of the intrusion. It is noteworthy that al-

Table 5. Confidence values allotted to each of the predictor maps used in the FIS modelling.

Predictor map	Confidence value	Justification
Euclidean distance to the Deccan LIP	0.9	The Deccan LIP is directly mapped in the field at 1 : 50 000 scale.
Euclidean distance to the Barmer rift (trace of Réunion mantle plume)	0.4	Interpreted map; the trace of the plume was derived based on the assumption that it coincides roughly with the Barmer–Cambay rift.
Euclidean distance to the Barmer rift	0.8	The rift was traced using magnetic data and inferred lineaments and further cross-verified with the traces published by Bladon et al. (2015a, b) and Dolson et al. (2015).
Euclidean distance to lineaments derived from magnetic data	0.8	Lineaments were mapped from high-resolution magnetic data.
Euclidean distance to lineaments derived from gravity data	0.6	Lineaments were mapped from low-resolution gravity data.
Euclidean distance to inferred faults	0.5	The faults are inferred, not directly mapped.
Euclidean distance to post-Cambrian, non-felsic intrusives	0.8	Exposed intrusions directly mapped in the field at 1 : 50 000 scale.
Euclidean distance to circular features	0.5	Circular features were mapped from high-resolution magnetic, low-resolution gravity and topographic data.
Euclidean distance to surficial lineaments derived from geophysical data	0.7	Lineaments were mapped from high-resolution magnetic and low-resolution gravity data.
Euclidean distance to intersections of surficial lineaments derived from geophysical data	0.7	Lineaments were mapped from high-resolution magnetic and low-resolution gravity data.
Magnetic anomaly map	0.9	Anomalies mapped from high-resolution magnetic data.

Table 6. Matrix summarising the target areas quantified according to probability and confidence levels, and recommended exploration. Target serial numbers refer to the rectangle numbers in Fig. 5a–c.

Target	Prospectivity	Probability	Confidence	Interpretation	Recommendation
Known carbonatite occurrences of Sarnu-Dandeli, Kamthai and Mundwara (green numbers 1, 3 and 4, respectively in Fig. 5a–c) and several areas surrounding them	High	High	High	High prospectivity because of the possible presence of extended branching conduits of the central carbonatite–alkaline complex intrusion	Apply direct detection techniques such as detailed geological mapping, high-resolution airborne radiometric surveys and drilling to identify mineral deposits.
(1) Circular region east of Sarnu-Dandeli (Fig. 5a and b; rectangle number 1); and A small area just south of the circular region (within rectangle 1 in Fig. 5a–c).	High	Moderate to high	High	The circular region represents the Siwana ring intrusion, consisting of alkali granites and rhyolites. High prospectivity may result from the consistent presence of lineaments and magnetic response of the intrusion.	Follow-up detailed exploration using high-resolution airborne radiometric surveys and ground geological mapping and geochemical sampling of outcrops, especially of the area south of the Siwana ring complex.
(2) Small area south of Barmer town	High	High	Moderate	High prospectivity because of the intersection of lineaments	Detailed geological mapping and aerial radiometric surveys are recommended, followed by high-resolution ground gravity surveys and later drilling if the radiometric surveys yield positive results.
(3) North of the Sarnu-Dandeli carbonatite occurrence	High	Moderate	High	High prospectivity because of the high density of lineaments and high magnetic anomalies.	Detailed geological mapping, high-resolution ground gravity and aerial radiometric surveys are recommended, followed by ground sampling and drilling if the radiometric and gravity surveys yield positive results.
(4) Northeast of the Sarnu-Dandeli carbonatite occurrence	High	Moderate	Moderate		
(5) Several areas east and southeast of Mundwara carbonatite occurrence	High	High	High	High prospectivity because of consistent overlap of lineaments derived from each geophysical source	Additional data collection – Geological mapping, high-resolution ground gravity, aerial radiometric surveys and geochemical sampling of outcrops to delineate deposits.

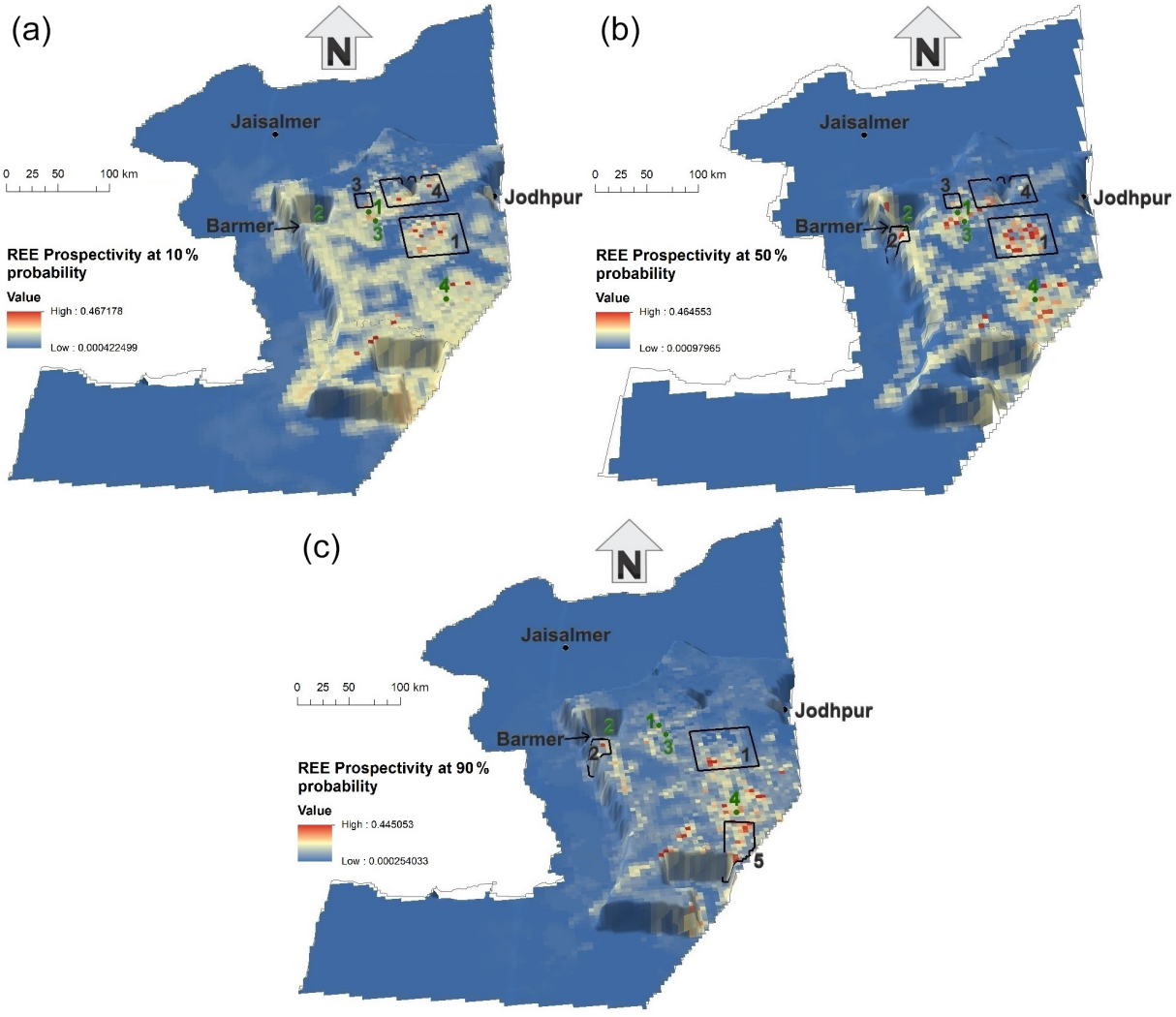

Figure 5. Continuous-scale prospectivity maps at 10 %, 50 % and 90 % probability levels draped over the confidence layer, shown in **(a)**, **(b)** and **(c)**, respectively. The colours mark increasing prospectivity from low (blue) to high (red). The elevations mark high confidence in the data used for prospectivity modelling. Black balls indicate major cities, and green balls indicate known carbonatite occurrences; green numbers correspond to the known carbonatite occurrences: 1 – Sarnu-Dandeli, 2 – Danta-Langera-Mahabar, 3 – Kamthai, 4 – Mundwara. Areas marked with black numbered rectangles are discussed in Sect. 7.

though it is not a carbonatite–alkaline complex, the peralkaline Siwana ring complex does contain REE potential and has been assessed for REE mineralisation (Bhushan and Somani, 2019). Further assessment of this region is recommended, with detailed radiometric surveys, geological mapping and geochemical sampling, especially of the area south of the Siwana ring complex that has high prospectivity at high probability levels.

A small area south of Barmer has high prospectivity at high probability and moderate confidence levels (Fig. 5b and c; rectangle number 2). This area has high prospectivity due to the intersection of lineaments. Two more areas to the north and northeast of the Sarnu-Dandeli carbonatite occurrence have high prospectivity at moderate probability and confidence levels (Fig. 5a and b, rectangles 3 and 4, respectively). A high density of lineaments and high magnetic anomalies are the likely causes. Detailed geological mapping and aerial radiometric surveys are recommended at all three locations, followed by ground sampling and drilling if the radiometric surveys yield positive results.

Several areas east and southeast of Mundwara have high prospectivity at high probability and confidence levels (Fig. 5c; rectangle 5). This is likely due to the consistent overlap of lineaments derived from each geophysical source at these locations. Acquiring additional data such as detailed geological maps, ground gravity and aerial radiometric surveys would help in delineating the target zone in these areas.

The emplacement of carbonatite–alkaline complexes in the study area was related to the large-scale rifting and splitting of India from Madagascar and later from the Seychelles, which also triggered Deccan volcanism. A similar mode of origin is envisaged for several other carbonatite–alkaline complexes worldwide. Ernst and Bell (2010) have identified several carbonatite provinces that are emplaced in an extensional setting, associated with a mantle plume and a LIP. These include, along with the Deccan province, the Afar province (eastern Africa), Paraná–Etendeka (South America and Africa), Siberian province (Russia), East European Craton–Kola province (eastern Europe), Central Iapetus province (North America, Greenland and the Baltic region), and pan-superior province (North America). The methodologies described in this paper can be used for exploration targeting REEs in these provinces.

Furthermore, at the time of emplacement of these carbonatite–alkaline complexes, the Indian subcontinent was located close to Madagascar and the Seychelles. Therefore, similar complexes could occur in Madagascar and the Seychelles also. The Barmer rift is the northern extension of the Cambay rift, which forms a triple junction in western India along with the Kutch rift. Thus, carbonatite–alkaline complexes are also expected along the Cambay rift and Kutch rifts, also possibly along the offshore E–W-trending Gop and the NNW–SSE-trending West Coast rift zones on the western coast of India. Kala–Dongar (Sen et al., 2016) and Murud–Janjira (Sethna and D'Sa, 1991) are known minor occurrences of carbonatites along the Kutch and West Coast rift zone, respectively. Moreover, the Gop rift is the western extension of the Son–Narmada–Tapti (SONATA) rift zone, along which several significant occurrences of the Chhota–Udepur carbonatite district are found. A similar study may help in identifying exploration targets for REEs in these regions. Paleo-reconstruction of the geography at the time when these complexes were being emplaced and analysing the prospectivity of the entire Deccan province (including western India, Madagascar and the Seychelles) may help identify more prospective targets for carbonatite-related REEs.

8 Summary, conclusions and recommendations

Rare earth elements comprise 17 metallic elements that are considered as "critical metals" for future development of environmentally friendlier and technologically based societies. India's production entirely comes from secondary beach placer deposits on the western and eastern coasts. Even though just one primary economic-grade deposit of REE is identified in India, there is significant latent potential for carbonatite-related REE deposits. This study has developed a knowledge-driven, GIS-based prospectivity model for exploration targeting of REEs associated with carbonatite–alkaline complexes in the western Rajasthan, northwestern India.

The generalised mineral systems model for carbonatite–alkaline-complex-related REEs described by Aranha et al. (under review) was used to identify regional-scale targeting criteria for REEs in the study area. Several predictor maps were derived from public-domain geological, geophysical and satellite data based on the mineral systems model. A multi-stage FIS was constructed to represent the different components of the mineral system. The first stage of the multi-stage FIS comprises three individual FISs to represent (1) plume-metasomatised SCLM in an extensional regime that make up fertile source regions for REE-bearing fluids and favourable geodynamic settings, (2) trans-lithospheric structures that provide favourable lithospheric architecture for the transportation of REE-enriched carbonatite–alkaline magma, and (3) near-surface higher-order structures that make up a shallow crustal architecture facilitating emplacement of carbonatite–alkaline complexes.

Systemic uncertainties associated with the fuzzification of the predictor maps was quantified based on the procedure described by Lisitsin et al. (2014) and Chudasama et al. (2017) that produced prospectivity maps at 10 %, 50 % and 90 % confidence levels. Stochastic uncertainties associated with the primary data used and the processing methods adopted to derive predictor maps were quantified based on the procedure described by Porwal et al. (2003), producing a confidence layer over which the prospectivity maps were draped.

Based on the results, a structural control over the emplacement of carbonatite–alkaline complexes is clearly recognised. The following are the recommendations based on the results of this study. Detailed project-scale ground exploration is recommended for the Kamthai–Sarnu-Dandeli and Mundwara regions and their immediate surroundings, where areas of high prospectivity are mapped at high probability levels. Exploration of the Siwana ring complex is recommended, particularly for the high prospectivity region to its south. Detailed geological mapping, high-resolution ground gravity and aerial radiometric surveys should be carried out in the regions to the north and northeast of Sarnu-Dandeli, south of Barmer, and the south of Mundwara to better resolve and delineate targets for ground exploration.

The prospectivity-analysis workflow presented in this paper can be applied to other geodynamically similar regions globally for targeting geological provinces for follow-up exploration such as the Deccan province, the Afar province (eastern Africa), Paraná–Etendeka (South America and Africa), Siberian province (Russia), East European Craton–Kola province (eastern Europe), Central Iapetus province (North America, Greenland and the Baltic region), and pan-superior province (North America).

Appendix A

Table A1. Location, physiography and geological setting of carbonatite–alkaline complexes in NW India.

Complex/district	Location and physiography	Regional geological setting	Remarks	Key references
Sarnu-Dandeli (25.614, 71.884) Danta-Langera-Mahabar (25.73, 71.42; Location and presence uncertain)	– Barmer district, Rajasthan state – located on the eastern shoulder of the Barmer Basin. – Carbonatites occur as dykes and veins varying from a few cm to about 12 m in length and from a few mm to about 30 cm in width cutting across the mafic alkaline rocks of the complex – Carbonatite dykes up to 12 m in length and 30 cm thick are found at Danta-Langera-Mahabar (similar to Sarnu-Dandeli)	– occurs within the Barmer continental rift basin – intrudes the Neoproterozoic rhyolitic rocks of the Malani Igneous province and Cretaceous sandstones and siltstones that are underlain by a basaltic flow – Barmer rift basin contains thick Mesozoic sediments that contain significant hydrocarbon reserves that are being actively exploited – Barmer and the Cambay basins have formed during Late Cretaceous in response to far-field stresses related to the Gondwana plate reorganisations that led to the formation of the 600 km long intracontinental rift.		Chandrasekaran (1987); Chandrasekaran and Chawade (1990); Chandrasekaran et al. (1990); Ray et al. (2000); Vijayan et al. (2016); Sheth et al. (2017)
Kamthai (25.633, 71.931)	– Located in the eastern edge of the Sarnu-Dandali complex in the Barmer Basin. – Highly enriched in REE and is considered a potential world-class deposit. – Kamthai plug is ellipsoidal in shape, covering an area of 19 475 m^2. – Dykes and veins of carbonatites are associated. – Characteristic panther skin texture for the plug carbonatites and golden yellow colour and occasional elephant skin weathering for the dykes and sills has been noted.		– Total REE resources of 4.65 MT, including 0.66 MT (proven), 1.33 MT (probable) and 2.66 MT (possible), in the Kamthai plug at the average grade of 2.69 %. – Additional resources of 259 000 t from dykes, sills and veins. – Overall, a total of 4.91 MT of REE ore at an average grade of 2.97 %	Bhushan and Kumar (2013); Bhushan (2015)
Mer Mundwara (24.828, 72.537)	– Sirohi District, Rajasthan state consists of three laccolith type intrusive plutons, namely, – Musala, Mer and Toa. – Mer is the biggest intrusion consisting of a complete ring structure and is about 1.3 km in diameter. – Toa forms half a ring structure and is about 700 m in diameter. – Musala appears as a mound, about 500 m in diameter.	– Occurs in close vicinity of the Barmer continental rift – Intrudes into the Neoproterozoic Erinpura Granite		Ray et al. (2000); Pande et al. (2017)

Table A2. Fuzzy if–then rules used for generating fuzzy prospectivity maps for fertile sources and favourable geodynamics settings.

	Consequent (if part)							Antecedent (then part)			
1	**If**	plume head/rift is	proximal	and	LIP is	proximal	**then**	fertility/geodynamic setting prospectivity is	high		
2	**If**	plume head/rift is	not distal*	and	LIP is	not distal*	**then**	fertility/geodynamic setting prospectivity is	high		
3	**If**	plume head/rift is	distal	or	LIP is	distal	**then**	fertility/geodynamic setting prospectivity is	low		
4	**If**	plume head/rift is	intermediate	or	LIP is	not distal*	**then**	fertility/geodynamic setting prospectivity is	intermediate		
5	**If**	plume head/rift is	not distal*	or	LIP is	intermediate	**then**	fertility/geodynamic setting prospectivity is	intermediate		

Table A3. Fuzzy if–then rules used for generating fuzzy prospectivity maps for favourable lithospheric architecture for transportation of REE-enriched carbonatite–alkaline magma.

	Consequent (IF part)													Antecedent (then part)			
1	**If**	rift is	proximal	and	Lineaments derived from remote sensing are	proximal	and	Lineaments derived from Magnetic data are	proximal	and	Lineaments derived from gravity data are	proximal		**then**	Pathways prospectivity is	architecture	High
2	**If**	rift is	intermediate	and	Lineaments derived from remote sensing are	proximal	and	Lineaments derived from Magnetic data are	proximal	and	Lineaments derived from gravity data are	proximal		**then**	Pathways prospectivity is	architecture	High
3	**If**				Lineaments derived from remote sensing are	proximal	and	Lineaments derived from Magnetic data are	proximal	and	Lineaments derived from gravity data are	proximal		**then**	Pathways prospectivity is	architecture	High
4	**If**	rift is	distal	or	Lineaments derived from remote sensing are	distal	or	Lineaments derived from Magnetic data are	distal	or	Lineaments derived from gravity data are	distal		**then**	Pathways prospectivity is	architecture	low
5	**If**	rift is	intermediate	and	Lineaments derived from remote sensing are	intermediate	and	Lineaments derived from Magnetic data are	intermediate	and	Lineaments derived from gravity data are	intermediate		**then**	Pathways prospectivity is	architecture	Intermediate
6	**If**							Lineaments derived from Magnetic data are	proximal	and	Lineaments derived from gravity data are	proximal		**then**	Pathways prospectivity is	architecture	High
7	**If**	rift is	not distal*	and	Lineaments derived from remote sensing are	not distal*	and	Lineaments derived from Magnetic data are	proximal	and	Lineaments derived from gravity data are	proximal		**then**	Pathways prospectivity is	architecture	High
8	**If**	rift is	not distal*	and	Lineaments derived from remote sensing are	not distal*	and	Lineaments derived from Magnetic data are	proximal	and	Lineaments derived from gravity data are	not distal		**then**	Pathways prospectivity is	architecture	High

* "Not distal" includes all fuzzy sets other than the "distal" set. In this case, it includes both the "proximal" and "intermediate" fuzzy sets.

Table A4. Fuzzy if–then rules used for generating fuzzy prospectivity maps for favourable shallow crustal (near-surface) architecture for emplacement of alkaline–carbonatite complexes.

	Consequent (IF part)																			Antecedent (then part)		
1	**If**	Lineaments derived from remote sensing are	proximal	and	intrusions are	proximal	and	LIPs are	not distal	and	circular features are	proximal	and	surficial faults derived from geophysical data are	proximal	and	intersections of surficial faults derived from geophysical data are	proximal	and	magnetic anomalies are	high	**then**	Emplacement architecture prospectivity is	High
2	**If**	Lineaments derived from remote sensing are	proximal	and	intrusions are	not distal	and	LIPs are	not distal	and	circular features are	proximal	and	surficial faults derived from geophysical data are	proximal	and	intersections of surficial faults derived from geophysical data are	proximal	and	magnetic anomalies are	high	**then**	Emplacement architecture prospectivity is	High
3	**If**	Lineaments derived from remote sensing are	proximal	and										surficial faults derived from geophysical data are	proximal							**then**	Emplacement architecture prospectivity is	High
4	**If**	Lineaments derived from remote sensing are	distal	or	intrusions are	distal	or	LIPs are	distal	or	circular features are	distal	or	surficial faults derived from geophysical data are	distal	or	intersections of surficial faults derived from geophysical data are	distal	or	magnetic anomalies are	low	**then**	Emplacement architecture prospectivity is	low
5	**If**	Lineaments derived from remote sensing are	intermediate	and	intrusions are	intermediate	and				circular features are	intermediate	and	surficial faults derived from geophysical data are	intermediate	and	intersections of surficial faults derived from geophysical data are	intermediate	and	magnetic anomalies are	intermediate	**then**	Emplacement architecture prospectivity is	Intermediate
6	**If**										circular features are	proximal	and	surficial faults derived from geophysical data are	proximal	and	intersections of surficial faults derived from geophysical data are	proximal	and	magnetic anomalies are	high	**then**	Emplacement architecture prospectivity is	High
7	**If**										circular features are	distal	and	surficial faults derived from geophysical data are	distal	and	intersections of surficial faults derived from geophysical data are	distal	and	magnetic anomalies are	low	**then**	Emplacement architecture prospectivity is	low
8	**If**										circular features are	intermediate	and	surficial faults derived from geophysical data are	intermediate	and	intersections of surficial faults derived from geophysical data are	intermediate	and	magnetic anomalies are	intermediate	**then**	Emplacement architecture prospectivity is	intermediate
9	**If**																intersections of surficial faults derived from geophysical data are	proximal	and	magnetic anomalies are	high	**then**	Emplacement architecture prospectivity is	High
10	**If**																intersections of surficial faults derived from geophysical data are	intermediate	and	magnetic anomalies are	intermediate	**then**	Emplacement architecture prospectivity is	intermediate
11	**If**																intersections of surficial faults derived from geophysical data are	distal	and	magnetic anomalies are	low	**then**	Emplacement architecture prospectivity is	low

Data availability. The study mainly used public domain datasets that have been summarised in Table 1 and in Sect. 3.

Author contributions. MA and AP conceptualised the study. MA, AP and MS designed the methodology. MA and MS carried out the preprocessing and feature extraction. Formal analysis was carried out by MA, AP and IGA. The investigation was carried out by MA, AP and IGA. MA, AP, AM, and KR organised the resources. Data curation was carried out by MA, MS and AM. MA, AP, and IG wrote the paper.

Competing interests. The contact author has declared that neither they nor their co-authors have any competing interests.

Disclaimer. Publisher's note: Copernicus Publications remains neutral with regard to jurisdictional claims in published maps and institutional affiliations.

Special issue statement. This article is part of the special issue "State of the art in mineral exploration". It is a result of the EGU General Assembly 2020, 3–8 May 2020.

Acknowledgements. This paper benefited greatly from valuable discussions with Majid Keykhay-Hosseinpoor and Bijal Chudasama, for which they are thanked. Juan Alcade is thanked for putting together this special issue. We express our gratitude to Michael Anenburg, Gregor Partington and two anonymous reviewers for their excellent insights and comments that significantly improved the quality of this paper and the handling editor, Solveig Pospiech, for processing this paper. Bureau Gravimétrique International (BGI)/International Association of Geodesy is acknowledged for distributing the satellite gravity data.

Review statement. This paper was edited by Solveig Pospiech and reviewed by Gregor Partington and two anonymous referees.

References

Aitken, A. R. A., Joly, A., Dentith, M. C., Johnson, S. P., Thorne, A. M., and Tyler, I. M.: 3D architecture, structural evolution, and mineral prospectivity of the Gascoyne Province, Western Australia, Rep. Geol. Surv. West. Aust., 123, 2014.

Allegre, C. J., Birck, J. L., Capmas, F., and Courtillot, V.: Age of the Deccan traps using 187Re–187Os systematics, Earth Planet. Sc. Lett., 170, 197–204, 1999.

Amante, C. and Eakins, B. W.: ETOPO1: 1 arc – minute global relief model: procedures, data sources and analysis, NOAA Tech. Mem. NESDIS NGDC24, NOAA, National Geophysical Data Center, Boulder (Co), 2009.

Andersen, A. K., Clark, J. G., Larson, P. B., and Donovan, J. J.: REE fractionation, mineral speciation, and supergene enrichment of the Bear Lodge carbonatites, Wyoming, USA, Ore Geol. Rev., 89, 780–807, 2017.

Anenburg, M. and Mavrogenes, J. A.: Carbonatitic versus hydrothermal origin for fluorapatite REE-Th deposits: Experimental study of REE transport and crustal "antiskarn" metasomatism, Am. J. Sci., 318, 335–366, 2018.

Anenburg, M., Mavrogenes, J. A., Frigo, C., and Wall, F.: Rare earth element mobility in and around carbonatites controlled by sodium, potassium, and silica, Sci. Adv., 6, eabb6570, https://doi.org/10.1126/sciadv.abb6570, 2020.

Aranha, M., Porwal, A., and González-Álvarez, I.: Targeting REE deposits associated with carbonatite and alkaline complexes in northeast India, Ore Geol. Rev., in review, 2022.

Basu, A. R., Renne, P. R., DasGupta, D. K., Teichmann, F., and Poreda, R. J.: Early and late alkali igneous pulses and a high–3He plume origin for the Deccan flood basalts, Science, 261, 902–906, 1993.

Bell, K. and Simonetti, A.: Source of parental melts to carbonatites–critical isotopic constraints, Miner. Petrol., 98, 77–89, 2010.

Bell, K. and Tilton, G. R.: Probing the mantle: the story from carbonatites, Eos T. Am. Geophys. Un., 83, 273–277, 2002.

Bertrand, G., Billa, M., Cassard, D., Tourlière, B., Angel, J. M., and Tertre, F.: A new method to assess favorability of critical by-product commodities: application to rare earth elements in Europe, in: Mineral Prospectivity, current approaches and future innovations – Orléans, France, The Mineral Prospectivity, current approaches and future innovations conference, 24–26 October 2017, p. 17, 2017.

Bhushan, S. K.: Geology of the Kamthai rare earth deposit, J. Geol. Soc. India, 85, 537–546, 2015.

Bhushan, S. K. and Kumar, A.: First carbonatite hosted REE deposit from India, J. Geol. Soc. India, 81, 41–60, 2013.

Bhushan, S. K. and Mohanty, M.: Mechanics of intrusion and geochemistry of alkaline granites from Siwana, Barmer district, Rajasthan, Indian Journal of Earth Sciences, 15, 103–115, 1988.

Bhushan, S. K. and Somani, O. P.: Rare earth elements and yttrium potentials of Neoproterozoic peralkaline Siwana granite of Malani igneous suite, Barmer district, Rajasthan, J. Geol. Soc. India, 94, 35–41, 2019.

Binnemans, K., Jones, P. T., Blanpain, B., Van Gerven, T., Yang, Y., Walton, A., and Buchert, M.: Recycling of rare earths: a critical review, J Clean. Prod., 51, 1–22, 2013.

Bladon, A. J., Burley, S. D., Clarke, S. M., and Beaumont, H.: Geology and regional significance of the Sarnoo Hills, eastern rift margin of the Barmer Basin, NW India, Basin Res., 27, 636–655, 2015a.

Bladon, A. J., Clarke, S. M., and Burley, S. D.: Complex rift geometries resulting from inheritance of pre–existing structures: Insights and regional implications from the Barmer Basin rift, J. Struct. Geol., 71, 136–154, 2015b.

Boesche, N. K., Rogass, C., Lubitz, C., Brell, M., Herrmann, S., Mielke, C., Tonn, S., Appelt, O., Altenberger, U., and Kaufmann, H.: Hyperspectral REE (rare earth element) mapping of outcrops–applications for neodymium detection, Remote Sens.-Basel, 7, 5160–5186, 2015.

Bonham-Carter, G. F.: Geographic information systems for geoscientists-modelling with GIS, Computer Methods in the Geoscientists, 13, p.398, 1994.

Bonvalot, S., Balmino, G., Briais, A., Kuhn, M., Peyrefitte, A., Vales, N., Biancale, R., Gabalda, G., Reinquin, F., and Sarrailh, M.: World Gravity Map, Commission for the Geological Map of the World, edited by: BGI-CGMW-CNES-IRD, Paris, 2012.

Castellano, G., Castiello, C., Pasquadibisceglie, V., and Zaza, G.: FISDeT: Fuzzy inference system development tool, Int. J. Comput. Int. Sys., 10, 13–22, 2017.

Castor, S. B.: The Mountain Pass rare-earth carbonatite and associated ultrapotassic rocks, California, Can. Mineral., 46, 779–806, 2008.

Chakhmouradian, A. R. and Wall, F.: Rare earth elements: minerals, mines, magnets (and more), Elements, 8, 333–340, 2012.

Chakhmouradian, A. R., Reguir, E. P., Kressall, R. D., Crozier, J., Pisiak, L. K., Sidhu, R., and Yang, P.: Carbonatite-hosted niobium deposit at Aley, northern British Columbia (Canada): Mineralogy, geochemistry and petrogenesis, Ore Geol. Rev., 64, 642–666, 2015.

Chandra, J., Paul, D., Viladkar, S. G., and Sensarma, S.: Origin of the Amba Dongar carbonatite complex, India and its possible linkage with the Deccan Large Igneous Province, Geological Society, London, Special Publications, 463, 137–169, 2018.

Chandrasekaran, V.: Geochemistry of the basic, acid and alkaline intrusives and extrusives of Sarnu-Dandali area, District Barmer, Rajasthan, Unpublished Ph.D. Thesis, University of Rajasthan, Jaipur, India, 108, 1987.

Chandrasekaran, V. and Chawade, M. P.: Carbonatites of Barmer district, Rajasthan, Indian Minerals, 44, 315–324, 1990.

Chandrasekaran, V., Srivastava, R. K., and Chawade, M. P.: Geochemistry of the alkaline rocks of Sarnu-Dandali area, district Barmer, Rajasthan, India, Journal of Geological Society of India (Online archive from Vol 1 to Vol 78), 36, 365–382, 1990.

Chenet, A. L., Quidelleur, X., Fluteau, F., Courtillot, V., and Bajpai, S.: ^{40}K–^{40}Ar dating of the Main Deccan large igneous province: Further evidence of KTB age and short duration, Earth Planet. Sc. Lett., 263, 1–15, 2007.

Chudasama, B., Porwal, A., Kreuzer, O. P., and Butera, K.: Geology, geodynamics and orogenic gold prospectivity modelling of the Paleoproterozoic Kumasi Basin, Ghana, West Africa, Ore Geol. Rev., 78, 692–711, 2016.

Chudasama, B., Lisitsin, V. A., and Porwal, A. K.: Uncertainties in prospectivity analysis of surficial uranium mineral systems in Western Australia, in: Mineral Prospectivity, current approaches and future innovations – Orléans, France, The Mineral Prospectivity, current approaches and future innovations conference, 24–26 October 2017, p. 24, 2017.

Collier, J. S., Sansom, V., Ishizuka, O., Taylor, R. N., Minshull, T. A., and Whitmarsh, R. B.: Age of Seychelles–India break–up, Earth Planet. Sc. Lett., 272, 264–277, 2008.

Cordeiro, P. F., Brod, J. A., Dantas, E. L., and Barbosa, E. S.: Mineral chemistry, isotope geochemistry and petrogenesis of niobium-rich rocks from the Catalão I carbonatite-phoscorite complex, Central Brazil, Lithos, 118, 223–237, 2010.

Devey, C. W. and Stephens, W. E.: Deccan–related magmatism west of the Seychelles–India rift, in: Magmatism and the Causes of Continental Break–up, edited by: Storey B. C., Alabaster T., Pankhurst R. J., Geological Society, London, Special Publications, 68, 271–291, 1992.

Dolson, J., Burley, S. D., Sunder, V. R., Kothari, V., Naidu, B., Whiteley, N. P., Farrimond, P., Taylor, A., Direen, N., and Anantha krishnan, B.: The discovery of the Barmer Basin, Rajasthan, India, and its petroleum geology, The Association of American Petroleum Geologists Bulletin, 99, 433–465, 2015.

Duda, R., Gaschning, J., and Hart, P.: Model design in the prospector consultant system for mineral exploration, in: Expert Systems, In the Microelectronic Age, edited by: Michie, D., Edinburgh University Press, Edinburgh, 153–167, 1979.

Duda, R. O., Hart, P. E., Barrett, P., Gasching, J. G., Konolige, K., Reboh, R., and Slocum, J.: Development of the prospector consultation system for mineral exploration, Final Report, SRI Projects 5821 and 6415, Artificial Intelligence Center, SRI International, Menlo Park, p. 193, 1978.

Duda, R. O., Nilsson, N. J., and Raphael, B.: State of technology in artificial intelligence, in: Research Directions in Software Technology, edited by: Wegner, P., MIT, Cambridge, Mass, 729–749, 1980.

Duke, G. I.: Black Hills–Alberta carbonatite–kimberlite linear trend: Slab edge at depth?, Tectonophysics, 464, 186–194, 2009.

Duke, G. I., Carlson, R. W., Frost, C. D., Hearn Jr, B. C., and Eby, G. N.: Continent-scale linearity of kimberlite–carbonatite magmatism, mid-continent North America, Earth Planet. Sc. Lett., 403, 1–14, 2014.

Ekmann, J. M.: Rare earth elements in coal deposits–a prospectivity analysis, in: Adapted from poster presentations AAPG Easter Section meeting, Cleveland, Ohio, The AAPG Eastern Section meeting, 22–26 September 2012, 22–26, 2012.

Elliott, H. A. L., Wall, F., Chakhmouradian, A. R., Siegfried, P. R., Dahlgren, S., Weatherley, S., Finch, A. A., Marks, M. A. W., Dowman, E., and Deady, E.: Fenites associated with carbonatite complexes: A review, Ore Geol. Rev., 93, 38–59, 2018.

Ernst, R. E. and Bell, K.: Large igneous provinces (LIPs) and carbonatites, Miner. Petrol., 98, 55–76, 2010.

Ganerød, M., Torsvik, T. H., Van Hinsbergen, D. J. J., Gaina, C., Corfu, F., Werner, S., Owen–Smith, T. M., Ashwal, L. D., Webb, S. J., and Hendriks, B. W. H.: Palaeoposition of the Seychelles microcontinent in relation to the Deccan Traps and the Plume Generation Zone in Late Cretaceous–Early Palaeogene time, in: The formation and evolution of Africa: a synopsis of 3.8 Ga of Earth history, edited by: Van Hinsbergen, D. J. J., Buiter, S. J. H., Torsvik, T. H., Gaina, C., and Webb, S. J., Geological Society, London, Special Publications, 357, 229–252, 2011.

Garson, M. S. and Smith, W. C.: Chilwa Island, Nyasaland [Malawi]: Nyasaland Geological Survey Department, memoir 1, 1958.

Giovannini, A. L., Neto, A. C. B., Porto, C. G., Pereira, V. P., Takehara, L., Barbanson, L., and Bastos, P. H.: Mineralogy and geochemistry of laterites from the Morro dos Seis Lagos Nb (Ti, REE) deposit (Amazonas, Brazil), Ore Geol. Rev., 88, 461–480, 2017.

Gönenç, T.: Investigation of distribution of embedded shallow structures using the first order vertical derivative of gravity data, J. Appl. Geophys., 104, 44–57, 2014.

González-Álvarez, I., Porwal, A., Beresford, S. W., McCuaig, T. C., and Maier, W. D.: Hydrothermal Ni prospectivity analysis of Tasmania, Australia, Ore Geol. Rev., 38, 168–183, 2010.

González-Álvarez, I., Stoppa, F., Yang, X. Y., and Porwal, A.: Introduction to the Special Issue, Insights on Carbonatites and their Mineral Exploration approach: A Challenge towards Resourc-

ing Critical Metals, Ore Geol. Rev. Special Issue, 133, 104073, https://doi.org/10.1016/j.oregeorev.2021.104073, 2021.

Goodenough, K. M., Schilling, J., Jonsson, E., Kalvig, P., Charles, N., Tuduri, J., Deady, E. A., Sadeghi, M., Schiellerup, H., Müller, A., and Bertrand, G.: Europe's rare earth element resource potential: An overview of REE metallogenetic provinces and their geodynamic setting, Ore Geol. Rev., 72, 838–856, 2016.

Goodenough, K. M., Wall, F., and Merriman, D.: The rare earth elements: demand, global resources, and challenges for resourcing future generations, Natural Resources Research, 27, 201–216, 2018.

GSI and AMD: Strategic Plan for Enhancing REE Exploration in India, Geological Survey of India and Atomic Mineral Directorate for Exploration and Research, https://employee.gsi.gov.in/cs/groups/public/documents/document/b3zp/oda5/~edisp/dcport1gsigovi809087.pdf or https://www.amd.gov.in/WriteReadData/userfiles/file/GSI_AMD_Vision_Document_REE.pdf, 2020.

Gunn, P. J. and Dentith, M. C.: Magnetic responses associated with mineral deposits, AGSO Journal of Australian Geology and Geophysics, 17, 145–158, 1997.

Holden, E. J., Fu, S. C., Kovesi, P., Dentith, M., Bourne, B., and Hope, M.: Automatic identification of responses from porphyry intrusive systems within magnetic data using image analysis, J. Appl. Geophys., 74, 255–262, 2011.

Indian Bureau of Mines: Indian Minerals Yearbook 2018 (Part- III: Mineral Reviews), Rare Earths, 57, 24.1–24.7, https://ibm.gov.in/writereaddata/files/02182020103349Rare%20Earths_2018.pdf (last access: 5 March 2022), 2018.

Indian Bureau of Mines: Indian Minerals Yearbook 2019 (Part- III: Mineral Reviews), Rare Earths, 58, 24.1–24.10, https://ibm.gov.in/writereaddata/files/10012020172151RareEarth_2019_AR.pdf (last access: 5 March 2022), 2019.

International Union of Pure and Applied Chemistry (IUPAC): Nomenclature of Inorganic Chemicals – IUPAC Recommendations 2005, RSC Publishing, Cambridge, UK , pp. 377, ISBN 0 85404 438 8, 2005.

Jacobsen, B. H.: A case for upward continuation as a standard separation filter for potential-field maps, Geophysics, 52, 1138–1148, 1987.

Jaireth, S., Hoatson, D. M., and Miezitis, Y.: Geological setting and resources of the major rare-earth-element deposits in Australia, Ore Geol. Rev., 62, 72–128, 2014.

Johnson, N. L., Kotz, S., and Balakrishnan, N.: Chapter 25: Beta Distributions, in: Continuous univariate distributions, volume 2 (Vol. 289), John Wiley & sons, ISBN 978-0-471-58494-0, 1995.

Joly, A., Porwal, A., and McCuaig, T. C.: Exploration targeting for orogenic gold deposits in the Granites–Tanami Orogen: Mineral system analysis, targeting model and prospectivity analysis, Ore Geol. Rev., 48, 349–383, 2012.

Jones, A. P., Genge, M., and Carmody, L.: Carbonate melts and carbonatites, Rev. Mineral. Geochem., 75, 289–322, 2013.

Jones, R. M. and Hillis, R. R.: An integrated, quantitative approach to assessing fault-seal risk, AAPG Bull., 87, 507–524, 2003.

Keating, P. and Sailhac, P.: Use of the analytic signal to identify magnetic anomalies due to kimberlite pipes, Geophysics, 69, 180–190, 2004.

Kozlov, E., Fomina, E., Sidorov, M., Shilovskikh, V., Bocharov, V., Chernyavsky, A., and Huber, M.: The Petyayan-Vara carbonatite-hosted rare earth deposit (Vuoriyarvi, NW Russia), Mineral. Geochem. Mineral., 10, p. 73, 2020.

Kreuzer, O. P., Etheridge, M. A., Guj, P., McMahon, M. E., and Holden, D. J.: Linking mineral deposit models to quantitative risk analysis and decision-making in exploration, Econ. Geol., 103, 829–850, 2008.

Latham, A. G., Harding, K. L., Lapointe, P., Morris, W. A., and Balch, S. J.: On the lognormal distribution of oxides in igneous rocks, using magnetic susceptibility as a proxy for oxide mineral concentration, Geophys. J. Int., 96, 179–184, 1989.

Laznicka, P.: Giant metallic deposits: Future sources of industrial metals, Springer Science & Business Media, Springer-Verlag Berlin Heidelberg, ISBN 978-3-642-12405-1, 2006.

Le Bas, M. J.: Fenites associated with carbonatites, Can. Mineral., 46, 915–932, 2008.

Lisitsin, V. A., Porwal, A., and McCuaig, T. C.: Probabilistic fuzzy logic modelling: quantifying uncertainty of mineral prospectivity models using Monte Carlo simulations, Math. Geosci., 46, 747–769, 2014.

Mariano, A. N.: Economic Geology of Rare Earth Elements, Rev. Mineral., 21, 309–337, 1989.

McCuaig, T. C. and Hronsky, J. M.: The mineral system concept: the key to exploration targeting, Soc. Eco. Geo. Spc. Pub., 18, 153–175, 2014.

McCuaig, T. C., Porwal, A., and Gessner, K.: Fooling ourselves: recognizing uncertainty and bias in exploration targeting, Centre for Exploration Targeting Quarterly News, The University of Western Australia, Crawley Western Australia, 2, p. 1, 2009.

Mitchell, R. H.: Primary and secondary niobium mineral deposits associated with carbonatites, Ore Geol. Rev., 64, 626–641, 2015.

Morgenstern, R., Turnbull, R. E., Hill, M. P., Durance, P. M. J., and Rattenbury, M. S.: Rare Earth Element Mineral Potential in New Zealand, GNS Science Consultancy Report, 23, GNS Science, Lower Hutt (NZ), 2018.

Neave, D. A., Black, M., Riley, T. R., Gibson, S. A., Ferrier, G., Wall, F., and Broom-Fendley, S.: On the feasibility of imaging carbonatite-hosted rare earth element deposits using remote sensing, Econ. Geol., 111, 641–665, 2016.

Pande, K., Cucciniello, C., Sheth, H., Vijayan, A., Sharma, K. K., Purohit, R., Jagadeesan, K. C., and Shinde, S.: Polychronous (Early Cretaceous to Palaeogene) emplacement of the Mundwara alkaline complex, Rajasthan, India: ^{40}Ar–^{39}Ar geochronology, petrochemistry and geodynamics, Int. J. Earth Sci., 106, 1487–1504, 2017.

Pawlowski, R. S.: Preferential continuation for potential-field anomaly enhancement, Geophysics, 60, 390–398, 1995.

Pirajno, F.: Intracontinental anorogenic alkaline magmatism and carbonatites, associated mineral systems and the mantle plume connection, Gondwana Res., 27, 1181–1216, 2015.

Poletti, J. E., Cottle, J. M., Hagen-Peter, G. A., and Lackey, J. S.: Petrochronological constraints on the origin of the Mountain Pass ultrapotassic and carbonatite intrusive suite, California, J. Petrol., 57, 1555–1598, 2016.

Porwal, A. and Carranza, E. J. M.: Introduction to the Special Issue: GIS-based mineral potential modelling and geological data analyses for mineral exploration, Ore Geol. Rev., 71, 477–483, 2015.

Porwal, A., Carranza, E. J. M., and Hale, M.: Knowledge-driven and data-driven fuzzy models for predictive mineral potential mapping, Natural Resources Research, 12, 1–25, 2003.

Porwal, A., González-Álvarez, I., Markwitz, V., McCuaig, T. C., and Mamuse, A.: Weights-of-evidence and logistic regression modelling of magmatic nickel sulfide prospectivity in the Yilgarn Craton, Western Australia, Ore Geol. Rev., 38, 184–196, 2010.

Porwal, A., Das, R. D., Chaudhary, B., González-Álvarez, I., and Kreuzer, O.: Fuzzy inference systems for prospectivity modelling of mineral systems and a case-study for prospectivity mapping of surficial Uranium in Yeelirrie Area, Western Australia, Ore Geol. Rev., 71, 839–852, 2015.

Porwal, A. K.: Mineral potential mapping with mathematical geological models (Vol. 130), ITC PhD dissertation, Utrecht University, Enschede, the Netherlands, ISBN 90-6164-240-X, 2006.

Porwal, A. K. and Kreuzer, O. P.: Introduction to the special issue: mineral prospectivity analysis and quantitative resource estimation, Ore Geol. Rev., 38, 121–127, 2010.

Rajagopalan, S.: Analytic signal vs. reduction to pole: solutions for low magnetic latitudes, Explor. Geophys., 34, 257–262, 2003.

Ramakrishnan, M. and Vaidyanadhan, R.: Geology of India (Vol. 1), Geological society of India, Bangalore, 556, 2008.

Ray, J. S. and Pande, K.: Carbonatite alkaline magmatism associated with continental flood basalts at stratigraphic boundaries: cause for mass extinctions, Geophys. Res. Lett., 26, 1917–1920, 1999.

Ray, J. S. and Ramesh, R.: Evolution of carbonatite complexes of the Deccan flood basalt province: stable carbon and oxygen isotopic constraints, J. Geophys. Res.-Sol. Ea., 104, 29471–29483, 1999.

Ray, J. S., Ramesh, R., Pande, K., Trivedi, J. R., Shukla, P. N., and Patel, P. P.: Isotope and rare earth element chemistry of carbonatite–alkaline complexes of Deccan volcanic province: implications to magmatic and alteration processes, J. Asian Earth Sci., 18, 177–194, 2000.

Reddi, A. G. B. and Ramakrishna, T. S.: Bouguer gravity atlas of western Indian (Rajasthan–Gujarat) shield, Geological Survey of India, New Delhi, India, 1988.

Roy, A. B. and Jakhar, S.: Geology of Rajasthan (North West India) Precambrian to Recent, Scientific Publishers, Jodhpur, India, pp. 421, 2002.

Sadeghi, M.: Regional-scale prospectivity mapping on REE mineralization in Bergslagen district, Sweden, in: Mineral Prospectivity, current approaches and future innovations – Orléans, France, The Mineral Prospectivity, current approaches and future innovations conference, 24–26 October 2017, p. 61, 2017.

Sen, G., Hames, W. E., Paul, D. K., Biswas, S. K., Ray, A., and Sen, I. S.: Pre–Deccan and Deccan magmatism in Kutch, India: implications of new 40Ar/39Ar ages of intrusions, Special Publication, J. Geol. Soc. India, 6, 211–222, 2016.

Sethna, S. F. and D'Sa, C. P.: Occurrence of ijolite with veinlets of carbonatite in the Deccan Trap at Murud–Janjira, Maharashtra, India, J. Geol. Soc. India, 37, 257–263, 1991.

Sheth, H., Pande, K., Vijayan, A., Sharma, K. K., and Cucciniello, C.: Recurrent Early Cretaceous, Indo–Madagascar (89–86 Ma) and Deccan (66 Ma) alkaline magmatism in the Sarnu-Dandali complex, Rajasthan: ^{40}Ar–^{39}Ar age evidence and geodynamic significance, Lithos, 284, 512–524, 2017.

Simandl, G. J. and Paradis, S.: Carbonatites: related ore deposits, resources, footprint, and exploration methods, Applied Earth Science, 127, 123–152, 2018.

Simonetti, A., Bell, K., and Viladkar, S. G.: Isotopic data from the Amba Dongar carbonatite complex, west–central India: evidence for an enriched mantle source, Chemical Geology, 122, 185–198, 1995.

Simonetti, A., Goldstein, S. L., Schmidberger, S. S., and Viladkar, S. G.: Geochemical and Nd, Pb, and Sr isotope data from Deccan alkaline complexes–inferences for mantle sources and plume–lithosphere interaction, J. Petrol., 39, 1847–1864, 1998.

Singh, P. K., Rajak, P. K., Singh, M. P., Singh, V. K., Naik, A. S., and Singh, A. K.: Peat swamps at Giral lignite field of Barmer basin, Rajasthan, Western India: understanding the evolution through petrological modelling, International Journal of Coal Science & Technology, 3, 148–164, 2016.

Skirrow, R. G., Huston, D. L., Mernagh, T. P., Thorne, J. P., Duffer, H., and Senior, A.: Critical commodities for a high–tech world: Australia's potential to supply global demand, Geoscience Australia, Canberra, 2013.

Spandler, C., Slezak, P., and Nazari-Dehkordi, T.: Tectonic significance of Australian rare earth element deposits, Earth-Sci. Rev., 207, p. 103219, 2020.

Stoppa, F., Pirajno, F., Schiazza, M., and Vladykin, N. V.: State of the art: Italian carbonatites and their potential for critical-metal deposits, Gondwana Res., 37, 152–171, 2016.

Thomas, M. D., Ford, K. L., and Keating, P.: Review paper: Exploration geophysics for intrusion-hosted rare metals, Geophys. Prospect., 64, 1275–1304, 2016.

U.S. Geological Survey: Mineral commodity summaries 2021, U.S. Geological Survey, 200 p., https://doi.org/10.3133/mcs2021, 2021.

Van Gosen, B. S., Verplanck, P. L., Seal, R. R., II, Long, K. R., and Gambogi, J.: Rare-earth elements, chap. O (No. 1802-O), in: Critical mineral resources of the United States–Economic and environmental geology and prospects for future supply, edited by: Schulz, K. J., DeYoung Jr., J. H., Seal II, R. R., and Bradley, D. C., U.S. Geological Survey Professional Paper 1802p, Reston, VA, O1–O31, https://doi.org/10.3133/pp1802O, 2017.

Verplanck, P. L. and Hitzman, M.: Rare earth and critical elements in ore deposits (Vol. Reviews in Economic Geology 18), Littleton, Society of Economic Geologists, Colorado, 2016.

Verplanck, P. L. and Van Gosen, B. S.: Carbonatite and alkaline intrusion–related rare earth element deposits–a deposit model (No. 2011–1256), US Geological Survey, Reston, Virginia, 2011.

Vijayan, A., Sheth, H., and Sharma, K. K.: Tectonic significance of dykes in the Sarnu-Dandali alkaline complex, Rajasthan, northwestern Deccan Traps, Geosci. Front. 7, 783–791, 2016.

Wall, F.: Rare earth elements, in: Critical metals handbook, edited by: Gunn, A. G., Wiley, London, 312–339, 2014.

Wall, F.: Rare earth elements, Encyclopedia of Geology, second edn., 680–693, https://doi.org/10.1016/B978-0-08-102908-4.00101-6, Academic Press, 2021.

Woolley, A. R. and Bailey, D. K.: The crucial role of lithospheric structure in the generation and release of carbonatites: geological evidence, Mineral. Mag., 76, 259–270, 2012.

Woolley, A. R. and Kjarsgaard, B. A.: Carbonatite occurrences of the world: map and database, Open File 5796, Geological Survey of Canada, Ottawa, Ontario, 2008a.

Woolley, A. R. and Kjarsgaard, B. A.: Paragenetic types of carbonatite as indicated by the diversity and relative abundances of associated silicate rocks: evidence from a global database, Can. Mineral., 46, 741–752, 2008b.

Zheng, Y. F.: Metamorphic chemical geodynamics in continental subduction zones, Chem. Geol., 328, 5–48, 2012.

Zheng, Y. F.: Subduction zone geochemistry, Geosci. Front., 10, 1223–1254, 2019.

Zimmermann, R., Brandmeier, M., Andreani, L., Mhopjeni, K., and Gloaguen, R.: Remote sensing exploration of Nb-Ta-LREE-enriched carbonatite (Epembe/Namibia), Remote Sens.-Basel, 8, p. 620, 2016.